J|A|C|S ARTICLES

Published on Web 01/15/2010

Control of Charge Transfer in a Series of $Ru_2^{II,II}$/TCNQ Two-Dimensional Networks by Tuning the Electron Affinity of TCNQ Units: A Route to Synergistic Magnetic/Conducting Materials

Hitoshi Miyasaka,*,† Natsuko Motokawa,† Satoshi Matsunaga,†,⊥ Masahiro Yamashita,† Kunihisa Sugimoto,‡,¶ Tatsuya Mori,§ Naoki Toyota,§ and Kim R. Dunbar*,∥

Department of Chemistry, Graduate School of Science, Tohoku University, 6-3 Aramaki-Aza-Aoba, Aoba-ku, Sendai, Miyagi 980-8578, Japan, X-ray Research Laboratory, Rigaku Co. Ltd., 3-9-12 Matsubara-cho, Akishima, Tokyo 196-8666, Japan, Department of Physics, Graduate School of Science, Tohoku University, 6-3 Aramaki-Aza-Aoba, Aoba-ku, Sendai, Miyagi 980-8578, Japan, and Department of Chemistry, Texas A&M University, PO Box 30012, College Station, Texas 77842-3012

Received November 12, 2009; E-mail: miyasaka@agnus.chem.tohoku.ac.jp

Abstract: The isostructural series of two-dimensional (2-D) fishnet-type network compounds, $[\{Ru_2(O_2CCF_3)_4\}_2(TCNQR_x)]\cdot n(solv)$ ($R_x = H_4$, **1**; Br_2, **2**; Cl_2, **3**; F_2, **4**; F_4, **5**), has been synthesized from the reactions of a paddlewheel diruthenium(II, II) complex, $[Ru_2^{II,II}(O_2CCF_3)_4]$, and neutral TCNQ derivatives ($TCNQR_x$ = 2,3,5,6- or 2,5-halogen-substituted 7,7,8,8-tetracyanoquinodimethane) under anaerobic conditions. Corresponding Rh compounds **1-Rh**−**5-Rh**, which are diamagnetic and redox-inactive, were also synthesized for the purpose of comparison with **1**−**5**. According to the electron affinity of $TCNQR_x$, which is related to its first reduction potential, the Ru_2 series (**1**−**5**) has the requisite driving force for charge transfer from $[Ru_2^{II,II}(O_2CCF_3)_4]$ to $TCNQR_x$, which can lead to a mixed-valence state of $[\{Ru_2^{4.5+}\}(TCNQR_x^{\bullet -})\{Ru_2^{4.5+}\}]$ for the 2-D network. Such a charge (or electron) transfer results in magnetic exchange interactions between $[Ru_2]$ units ($S = 1$ for $[Ru_2^{II,II}]$ and $S = 3/2$ for $[Ru_2^{II,III}]^+$) via $TCNQR_x^{\bullet -}$ $S = 1/2$ radicals that lead to long-range magnetic ordering in the layer. In the present series, only **5** demonstrated the full electron transfer (1-e^- transfer) to the mixed-valence state, whereas other members are essentially in the state $[\{Ru_2^{4+}\}(TCNQR_x^0)\{Ru_2^{4+}\}]$. Whereas **1**−**4** are paramagnetic, **5** is a metamagnet undergoing 3-D long-range antiferromagnetic ordering at 95 K ($= T_N$) and reverts to a magnetic-field-induced ferromagnetic state exhibiting coercivity up to 60 K. This result is consistent with the fact that $TCNQF_4$ has the strongest electron affinity among the $TCNQR_x$ molecules. Even in neutral forms, however, **1**−**4** can be observed to undergo thermally and/or field-activated charge transfers from $[Ru_2^{II,II}]$ to $TCNQR_x$ to give semiconductors with an activation energy of 200−300 meV, which is a driving force to transport electrons over the lattice. As determined by their conducting properties, the ease of thermally and/or field-activated charge transfers is on the order of **1** < **4** < **2** ≈ **3** ≪ **5**, which is in agreement with the order of electron affinity of $TCNQR_x$. Indeed, a magnetic anomaly with short-range order associated with the localization of charge-transferred electrons was revealed in the low-temperature susceptibility data for **2** and **3**. Finally, **5** was subjected to terahertz time-domain spectroscopy, the data from which revealed that transport hopping electrons scattered at high temperatures interact with magnetically ordered spins with the scattering being suppressed at T_N, at which temperature the real part of the complex electronic conductivity (σ_1) and dielectric permeability (ε_1) are dramatically altered. From these collective data, we conclude that molecular design based on an interunit charge transfer in a paramagnetic lattice is an efficient route to the design of materials with synergism between magnetic and conducting properties.

Introduction

As research in materials chemistry continues to evolve, increasing attention is being paid to molecule-based high-temperature magnets and conducting materials. Design of materials in these two categories is typically driven by different philosophies, and historically they have been treated as separate fields in chemistry and physics. This situation has changed in recent years, however, and currently the design of magnetic-conducting molecular materials in which both properties are mutually coupled to act synergistically is recognized as a key challenge for chemists working in both fields.[1] In such materials, itinerant electrons are no longer isotropic entities but rather are anisotropic "spins", namely, electrons possessing spin degree of freedom by interacting with ordered magnetic spins. Such a situation allows one to imagine various applications such as new types of magnetoresistance materials, spin valves, or magnetic

† Department of Chemisty, Tohoku University.
‡ Rigaku Co. Ltd.
§ Department of Physics, Tohoku University.
∥ Texas A&M University.
⊥ Current address: Department of Chemistry, Faculty of Science, Kanagawa University, 2946 Tsuchiya, Hiratsuka, Kanagawa 259-1293, Japan.
¶ Current address: Japan Synchrotron Radiation Research Institute, Kouto, Mikazuki, Sayo-gun, Hyogo 679-5198, Japan.

(1) Coronado, E.; Epstein, A. J. *J. Mater. Chem.* **2009**, *19*, 1670.

10.1021/ja909489s

filters for spin electronics (referred to as spintronics) devices.[2,3] The question that arises is: how can one approach the design of such materials in *molecular* systems?

Given the remarkable progress of strategies based on self-aggregation of functional molecules,[4−6] direct fabrication of magnetic-conducting co-frameworks by self-assembly is a natural route. A key molecular platform for this approach is a class of charge-transfer complexes that forms covalently bonded frameworks. In this vein, we turned to charge-transfer complexes based on metal donors and organic acceptors that form metal-organic frameworks (MOFs). In the case of a one-electron (1-e^-) transfer, the 1:1 donor (D)/acceptor (A) alternating array will likely lead to a charge-polarized (ionic) state with localized spins,[7,8] whereas a 2:1 stoichiometry, with the units being essentially the same electronically, is poised to lead to a mixed-valence state between two D units owing to a resonance of [D^+-A^--D ↔ D-A-D ↔ D-A^--D^+] in D_2A systems and vice versa in A_2D systems (vide infra). Such a charge-transfer resonance is reminiscent of three pioneering donor−acceptor compounds: the pyrazine-bridged mixed-valence Ru complex [$(NH_3)_5$Ru-pyz-Ru$(NH_3)_5$]$^{5+}$ known as the Creutz-Taube ion and its derivatives,[9] which undergo a charge-transfer resonance of [Ru^{2+}-Ru^{3+} ↔ Ru^{3+}-Ru^{2+}] classified to Class II or III of the Robin−Day scale;[10] [$(NH_3)_5Ru^{III}$-Dycid-$Ru^{III}(NH_3)_5$]$^{4+}$ (Dycid^{2-} = 1,4-dicyanamidobenzenate) reported by Aquino et al.,[11] which exhibits a very strong magnetic interaction between the Ru^{III} centers ($S = 1/2$) with $J > 400$ cm^{-1} owing to a charge-transfer resonance of [A^--D^+-A ↔ A-D-A ↔ A-D^+-A^-] (A_2D system);

Scheme 1

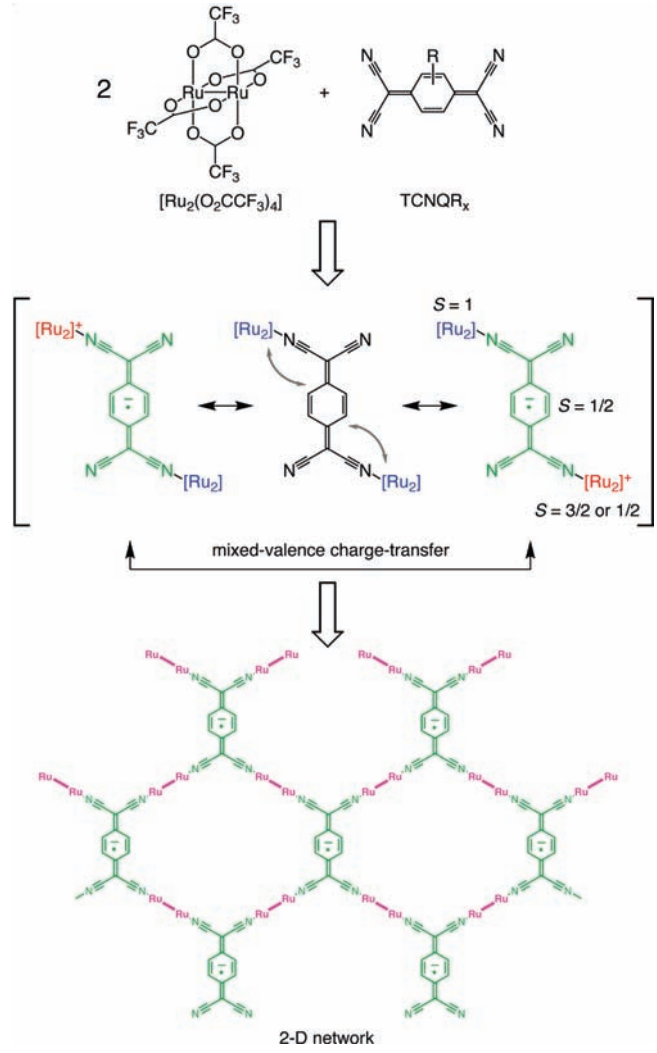

and [Cu^{II}(DCNQI)$_2$] and its derivatives,[12] which finally led to the realization of the ideal resonance scheme for a D_2A system that exhibits metallic properties. Furthermore, it is noteworthy that Wudl et al. expanded this concept to include organic radical arrays that behave as ferromagnetic organic metals[13] and that Sugawara et al. achieved a pure organic system that exhibits negative magnetoresistance.[14]

Our strategy for preparing 2:1 assemblies involves the use of electron-rich paddlewheel-type dimetal units and polycyano organic molecules (i.e., D_2A system), which yield favorable charge-transfer materials with M-L π-backbonding (Scheme 1). Specifically, a diruthenium(II, II) unit, [$Ru_2^{II,II}(O_2CCF_3)_4$] ($CF_3CO_2^-$ = trifluoroacetate),[15] possessing an $S = 1$ state emanating from the quasi-degenerate $2\pi^{*1}\delta^{*2}$ configuration of the Ru−Ru bond[16] and large anisotropy (zero-field splitting)

(2) (a) Prinz, G. A. *Science* **1998**, *282*, 1660. (b) Wolf, S. A.; Awschalom, D. D.; Buhrman, R. A.; Daughton, J. M.; von Molnár, S.; Roukes, M. L.; Chtchelkanova, A. Y.; Treger, D. M. *Science* **2001**, *294*, 1488. (c) Gregg, J. F.; Petej, I.; Jouguelet, E.; Dennis, C. *J. Phys. D: Appl. Phys.* **2002**, *35*, R121. (d) Tokura, Y. *Rep. Prog. Phys.* **2006**, *69*, 797.
(3) (a) Camarero, J.; Coronado, E. *J. Mater. Chem.* **2009**, *19*, 1678. (b) Wang, F.; Vardeny, Z. V. *J. Mater. Chem.* **2009**, *19*, 1685. (c) Sugawara, T.; Matsushita, M. M. *J. Mater. Chem.* **2009**, *19*, 1738.
(4) (a) Coronado, E.; Galán-Mascarós, J. R.; Gómez-Garcia, C. J.; Laukhin, V. *Nature* **2000**, *408*, 447. (b) Alberola, A.; Coronado, E.; Galán-Mascarós, J. R.; Giménez-Saiz, C.; Gómez-Garcia, C. J. *J. Am. Chem. Soc.* **2003**, *125*, 10774.
(5) (a) Coronado, E.; Day, P. *Chem. Rev.* **2004**, *104*, 5419. (b) Coronado, E.; Galán-Mascarós, J. R. *J. Mater. Chem.* **2005**, *15*, 66.
(6) (a) Takahashi, K.; Cui, H.-B.; Okano, Y.; Kobayashi, H.; Mori, H.; Tajima, H.; Einaga, Y.; Sato, O. *J. Am. Chem. Soc.* **2008**, *130*, 6688. (b) Clemente-Leon, M.; Coronado, E.; Giménez-López, M. C.; Soriano-Portillo, A.; Waerenborgh, J. C.; Delgado, F. S.; Ruiz-Pérez, C. *Inorg. Chem.* **2008**, *47*, 9111.
(7) (a) Candela, G. A.; Swartzendruber, L. J.; Miller, J. S.; Rice, M. J. *J. Am. Chem. Soc.* **1979**, *101*, 2755. (b) Miller, J. S.; Reis, A. H., Jr.; Gebert, E.; Ritsko, J. J.; Salaneck, W. R.; Kovnat, L.; Cape, T. W.; Van Duyne, R. P. *J. Am. Chem. Soc.* **1979**, *101*, 7111. (c) Broderick, W. E.; Thompson, J. A.; Day, E. P.; Hoffman, B. M. *Science* **1990**, *249*, 401. (d) Broderick, W. E.; Hoffman, B. M. *J. Am. Chem. Soc.* **1991**, *113*, 6334.
(8) (a) Miller, J. S.; Calabrese, J. C.; Rommelmann, H.; Chittipeddi, S. R.; Zhang, J. H.; Reiff, W. M.; Epstein, A. J. *J. Am. Chem. Soc.* **1987**, *109*, 769. (b) Yee, G. T.; Manriquez, J. M.; Dixon, D. A.; McLean, R. S.; Groski, D. M.; Flippen, R. B.; Narayan, K. S.; Epstein, A. J.; Miller, J. S. *Adv. Mater.* **1991**, *3*, 309. (c) Miller, J. S.; McLean, R. S.; Vazquez, C.; Calabrese, J. C.; Zuo, F.; Epstein, A. J. *J. Mater. Chem.* **1993**, *3*, 215. (d) Eichhorn, D., M.; Skee, D. C.; Broderick, W. E.; Hoffman, B. M. *Inorg. Chem.* **1993**, *32*, 491.
(9) (a) Creutz, C.; Taube, H. *J. Am. Chem. Soc.* **1969**, *91*, 3988. (b) Creutz, C.; Taube, H. *J. Am. Chem. Soc.* **1973**, *95*, 1086. (c) Tom, G. M.; Creutz, C.; Taube, H. *J. Am. Chem. Soc.* **1974**, *96*, 7827. (d) Powers, M. J.; Salmon, D. J.; Callahan, R. W.; Meyer, T. J. *J. Am. Chem. Soc.* **1976**, *98*, 6731.
(10) Robin, M. B.; Day, P. *Adv. Inorg. Chem. Radiochem.* **1967**, *10*, 247.
(11) Aquino, M. A. S.; Lee, F. L.; Gabe, E. J.; Bensimon, C.; Greedan, J. E.; Crutchley, R. J. *J. Am. Chem. Soc.* **1992**, *114*, 5130.
(12) (a) Aumüller, A.; Erk, P.; Klebe, G.; Hünig, S.; von Scütz, J. U.; Werner, H.-P. *Angew. Chem., Int. Ed. Engl.* **1986**, *25*, 740. (b) Kato, R.; Kobayashi, H.; Kobayashi, A. *J. Am. Chem. Soc.* **1989**, *111*, 5224.
(13) Dormann, E.; Nowak, M. J.; Williams, K. A.; Angus, Jr, R. O.; Wudl, F. *J. Am. Chem. Soc.* **1987**, *109*, 2594.
(14) Matsushita, M. M.; Kawakami, H.; Sugawara, T. *Phys. Rev. B* **2008**, *77*, 195208.
(15) Lindsay, A. J.; Wilkinson, G.; Motevalli, M.; Hursthouse, M. B. *J. Chem. Soc., Dalton Trans.* **1987**, 2723.
(16) Clark, D. L.; Green, J. C.; Redfern, C. M. *J. Chem. Soc., Dalton Trans.* **1989**, 1037.

with $D \approx 270$ cm^{-1} was chosen as a donor unit.[17] This molecule can be isolated and reversibly oxidized by 1-e$^-$ to give $[Ru_2^{II,III}(O_2CCF_3)_4]^+$, which exists in the $S = 3/2$ state ($2\pi^{*1}\delta^{*1}$) with $D \approx 60$ cm^{-1}.[18] The diruthenium units act as a linear-type coordination-acceptor building block for the construction of functional MOFs. Derivatives of the molecule 7,7,8,8-tetracyano-*p*-quinodimethane (TCNQ) derivatives (abbreviated as $TCNQR_x$, where R is the substituent and x is the number of them) were chosen as the acceptor units because of their demonstrated ability to form the stable 1-e$^-$-reduced form ($TCNQR_x^{\bullet -}$) with $S = 1/2$ (they are also capable of accepting a second electron if the reducing agent is sufficiently strong) and to act as a μ_4-ligand to the $[Ru_2]$ units. Conventionally, the trend of electron affinity of $TCNQR_x$ can be approximated by the first redox potential ($E_{1/2}$) in solution:[19,20] TCNQ ($E_{1/2} = -54$ mV) < $TCNQF_2$ ($E_{1/2} = 165$ mV) < $TCNQCl_2$ ($E_{1/2} = 191$ mV) ≈ $TCNQBr_2$ ($E_{1/2} = 194$ mV) < $TCNQF_4$ ($E_{1/2} = 365$ mV) ($E_{1/2}$ vs Ag/Ag^+ in CH_2Cl_2; $E_{1/2}$ for $Fc/Fc^+ = 219$ mV; $TCNQBr_2$ = 2,5-dibromo-7,7,8,8-tetracyanoquinodimethane; $TCNQCl_2$ = 2,5-dichloro-7,7,8,8-tetracyanoquinodimethane; $TCNQF_2$ = 2,5-difluoro-7,7,8,8-tetracyanoquinodimethane; $TCNQF_4$ = 2,3,5,6-tetrafluoro-7,7,8,8-tetracyanoquinodimethane). Although ladder-type chains[21] and 3-D networks[22] have been isolated in a few cases, the reactions mainly lead to a 2-D neutral network with a 2:1 stoichiometry (Scheme 1),[23] with the interunit charge transfer inducing a resonance that allows for long-range coupling of spins that is required for magnetic ordering and charge/electron transport.

Herein we report a systematic investigation of an isostructural series of 2:1 combinations of $[Ru_2^{II,II}(O_2CCF_3)_4]$ and the TCNQ derivatives ($TCNQR_x$); $[\{Ru_2^{II,II}(O_2CCF_3)_4\}_2(TCNQR_x)]$ ($TCNQR_x$ = TCNQ, **1**;[24] $TCNQBr_2$, **2**; $TCNQCl_2$, **3**; $TCNQF_2$, **4**; $TCNQF_4$, **5**[25]). The aim is to correlate charge transfer with magnetic ordering and electronic conductivity. For the sake of comparison with this series, corresponding isomorphous compounds with $[Rh_2^{II,II}(O_2CCF_3)_4]$ (**1-Rh**−**5-Rh**), which do not experience charge transfer due to disparate redox properties, were also prepared and fully characterized. The electron affinity of the $TCNQR_x$ acceptor unit tunes the charge transfer from $[Ru_2^{II,II}(O_2CCF_3)_4]$ to $TCNQR_x$ and consequently strongly affects the bulk magnetic and conducting properties. Finally, we report charge transfer in **5** to give a fully reduced $TCNQF_4^{\bullet -}$ ligand, which provides a proof of concept for coupling between magnetic ordered spins and electrons probably associated with hopping transport. The magnetic and conducting properties of **1**−**5** affected by charge transfer between $[Ru_2]$ and $TCNQR_x$ in a layer are discussed, and the concept of the present design strategy to achieve synergy between magnetic and conducting properties is elaborated.

Results and Discussion

Syntheses. Compound **1** was synthesized previously by refluxing a mixture of $[Ru_2^{II,II}(O_2CCF_3)_4(THF)_2]$ and TCNQ in toluene. The product was obtained mostly as a powder sample with a small amount of admixed crystals in the filtrate (the sample was characterized as a formula of **1**·3(toluene)).[24] To obtain quantitative amounts of homogeneous crystals and to find conditions that could be generalized for use with other TCNQ derivatives, the original synthesis was modified by a method that involves slow diffusion of a three-composite layer consisting of bottom/middle/top = $TCNQR_x$ in CH_2Cl_2/CH_2Cl_2+toluene/$[Ru_2]$ in toluene. This method leads solely to the formation of block-type crystals of **1**·3(toluene) and is also successful when *p*-xylene and 4-chlorotoluene (4-Cltoluene) is used instead of toluene for the $[Ru_2^{II,II}(O_2CCF_3)_4]$ layer, which leads to **1**·3(*p*-xylene)[25] and **1**·3(4-Cltoluene), respectively. It is important to point out that the use of a narrow diameter glass tube with less than 8 mm for the 4-Cltoluene/CH_2Cl_2 diffusion experiment leads to the formation of a ladder-type chain motif that is different than the 2-D layered compound with the same stoichiometry of $[\{Ru_2(O_2CCF_3)_4\}_2(TCNQ)]$ (however, this compound is a needle-type crystal and distinguishable by its crystal shape).[21] Compounds **2**−**5** were thus synthesized by employing this diffusion method with *p*-xylene in the $[Ru_2^{II,II}(O_2CCF_3)_4]$ layer. If not otherwise specified, **1**− **5** mean **1**·3(*p*-xylene), **2**·*p*-xylene·$2CH_2Cl_2$, **3**·1.2(*p*-xylene)·$2CH_2Cl_2$, **4**·2.3(*p*-xylene)·$1.4CH_2Cl_2$, and **5**·3(*p*-xylene) hereafter. The Rh derivatives (**1-Rh**−**5-Rh**) were synthesized in an identical manner using $[Rh_2^{II,II}(O_2CCF_3)_4]$ instead of $[Ru_2^{II,II}(O_2CCF_3)_4(THF)_2]$.

Structural Characterization of 1−**5.** Except for **3** because of its intricate twinning issues, all compounds were characterized by single-crystal X-ray crystallography (Table 1). The structure of **3** was confirmed by X-ray powder diffraction (lattice parameters were refined using the LeBail method;[26] vide infra). Thermal ellipsoid drawings of the basic formula units of **1**, **2**, **4**, and **5** are depicted in Figure 1. Selected bond distances around the Ru_2 unit are listed in Table S1 in Supporting Information. All compounds crystallize in the monoclinic *C*2/*m* with an inversion center located at the midpoint of the Ru−Ru bond and a set of C_2 axis and a mirror plane that intersect the $TCNQR_x$ ($Z = 2$) units, which leads to disorder of the R_x (Br_2 and F_2) substituents with an occupancy of 0.5 per site. This high symmetry leads to one $[Ru_2(O_2CCF_3)_4]$ and TCNQ unit with only one unique $Ru-N_{N\equiv C}$ bond in an asymmetric unit, although the stoichiometry is 2:1. The $Ru-N_{N\equiv C}$ bond lengths in **1**, **2**, **4**, and **5** are 2.284(2), 2.233(14), 2.291(3), and 2.260(4) Å, respectively, and the Ru−N−C angles are nearly linear (170−176°). The two axial sites of the $[Ru_2]$ units are occupied by N≡C- groups of $TCNQR_x$ to yield a 2-D fishnet-like hexagonal network (Figure 2a for **5**). The stacking feature of the 2-D layers is very similar among these compounds (Figure 2b for **5**), but their interlayer distances are different. The stacking direction is along the *a*-*c* direction, so the interlayer distance is closely related to the lengths of the *a* and *c* axes of the unit cell, but the *a* axis parameter is more indicative than the *c* axis for reflecting the interlayer distance; the longest *a* axis is found

(17) Dikarev, E. V.; Filatov, A. S.; Clérac, R.; Petrukhina, M. A. *Inorg. Chem.* **2006**, *45*, 744.
(18) Cotton, F. A.; Matusz, M.; Zhong, B. *Inorg. Chem.* **1988**, *27*, 4368.
(19) Saito, G.; Yoshida, Y. *Bull. Chem. Soc. Jpn.* **2007**, *80*, 1.
(20) Horiuchi, S.; Kumai, R.; Okimoto, Y.; Tokura, Y. *Chem. Phys.* **2006**, *325*, 78.
(21) Motokawa, N.; Oyama, T.; Matsunaga, S.; Miyasaka, H.; Sugimoto, K.; Yamashita, M.; Lopez, N.; Dunbar, K. R. *Dalton Trans.* **2008**, 4099.
(22) Motokawa, N.; Miyasaka, H.; Yamashita, M.; Dunbar, K. R. *Angew. Chem., Int. Ed.* **2008**, *47*, 7760.
(23) Motokawa, N.; Oyama, T.; Matsunaga, S.; Miyasaka, H.; Yamashita, M.; Dunbar, K. R. *CrystEngComm* **2009**, *11*, 2121.
(24) Miyasaka, H.; Campos-Fernández, C. S.; Clérac, R.; Dunbar, K. R. *Angew. Chem., Int. Ed.* **2000**, *39*, 3831.
(25) Miyasaka, H.; Izawa, T.; Takahashi, N.; Yamashita, M.; Dunbar, K. R. *J. Am. Chem. Soc.* **2006**, *128*, 11358.
(26) Le Bail, A.; Duroy, H.; Fourquet, J. L. *Mater. Res. Bull.* **1998**, *23*, 447.

Table 1. Crystallographic Data for **1**, **2**, **4**, and **5** and **1-Rh**, **4-Rh**, and **5-Rh**

	1·3(*p*-xylene)	**1-Rh**·3(*p*-xylene)	**2**·*p*-xylene·2CH_2Cl_2	**4**·2.3(*p*-xylene)·1.4CH_2Cl_2	**4-Rh**·2.7(*p*-xylene)·0.6CH_2Cl_2	**5**·3(*p*-xylene)	**5-Rh**·*p*-xylene·4CH_2Cl_2
formula	$C_{52}H_{34}F_{24}N_4O_{16}Ru_4$	$C_{52}H_{34}F_{24}N_4O_{16}Rh_4$	$C_{38}H_{16}Br_2Cl_4F_{24}N_4O_{16}Ru_4$	$C_{47.8}H_{27.8}Cl_{2.8}F_{26}N_4O_{16}Ru_4$	$C_{50.2}H_{30.2}Cl_{1.2}F_{26}N_4O_{16}Rh_4$	$C_{52}H_{30}F_{28}N_4O_{16}Ru_4$	$C_{40}H_{18}Cl_8F_{28}N_4O_{16}Rh_4$
formula weight	1831.10	1838.44	1946.42	1911.67	1893.53	1903.06	2037.80
color, shape	green, prism	purplish-brown, platelet	greenish-brown, chip	dark green, prism	greenish-purple, prism	greenish-blue, prism	greenish-purple, prism
crystal system	monoclinic	monoclinic	monoclinic	monoclinic	monoclinic	monoclinic	monoclinic
space group	*C*2/*m* (No. 12)	*C*2/*m* (No. 12)	*C*2/*m* (No. 12)	*C*2/*m* (No. 12)	*C*2/*m* (No. 12)	*C*2/*m* (No. 12)	$P2_1/c$ (No. 14)
T/K	93(1)	103(1)	93(1)	103(1)	103(1)	117(1)	93(1)
a/Å	16.7809(8)	16.825(3)	20.058(2)	17.402(10)	17.555(7)	17.542(14)	8.734(4)
b/Å	20.8853(10)	20.753(4)	20.031(2)	20.705(10)	20.578(8)	20.644(16)	20.410(8)
c/Å	8.7101(4)	8.5773(15)	8.5425(10)	8.722(5)	8.505(4)	8.788(7)	17.895(8)
β/deg	95.594(3)	95.607(3)	99.986(7)	95.629(8)	95.622(7)	96.627(13)	96.128(6)
V/Å^3	3038.1(2)	2980.6(9)	3380.3(6)	3127(3)	3057(2)	3161(4)	3172(2)
Z	2	2	2	2	2	2	2
D_{calc}/g·cm^{-3}	2.001	2.048	1.912	2.030	2.057	1.999	2.134
F_{000}	1788.00	1796.00	1860.00	1856.40	1843.60	1852.00	1964.00
no. of reflections	13634	12071	5127	12206	12261	14607	24050
no. of observations	3205	3423	5127	3638	2768	3327	5462
no. of variables	253	236	231	263	236	261	460
μ (Mo Kα)/cm^{-1}	11.202	12.329	23.437	12.127	12.603	10.894	15.038
GOF	1.000	1.074	1.099	1.019	1.002	1.018	1.011
$R1^a$ ($I > 2.00\sigma(I)$)	0.0452	0.0381	0.1119	0.0380	0.0691	0.0681	0.0557
$wR2^a$ (all data)	0.0462	0.0471	0.1560	0.0554	0.0963	0.0961	0.0790
$wR2^b$ (all data)	0.1523	0.0945	0.2893	0.0880	0.2026	0.1286	0.1374
ρ_{max}/e$^-$ Å^{-3}	3.74	1.22	0.93	2.18	3.36	2.11	2.70
ρ_{min}/e$^-$ Å^{-3}	−1.37	−0.66	−0.89	−1.35	−1.34	−1.12	−1.62

^{a} $R1 = \sum||F_o| - |F_c||/\sum|F_o|$. ^{b} $wR2 = [\sum w(F_o^2 - F_c^2)^2/\sum w(F_o^2)^2]^{1/2}$.

in **2** with 20.058(2) Å and the shortest one is **1** with 16.7809(8) Å (the trend of the distance is **1** < **4** < **5** < **2** as can be seen in Table 1). The interlayer distances of **1**, **2**, **4**, and **5**, defined by the distance between the least-squares planes, are 6.0, 7.1, 6.4, and 6.6 Å, respectively, and the trend is **1** < **4** < **5** < **2**. The structural similarity of **3** with other compounds was confirmed by comparing the XRPD patterns depicted in Figure S1 in Supporting Information, which reveal that the pattern of **3** is very similar to that of **2**, indicating their structural similarity. The unit cell of **3** was determined to be $a = 20.124(2)$ Å, $b = 20.130(2)$ Å, $c = 8.6665(7)$ Å, $\beta = 100.227(6)°$ with *C*2/*m* ($R_p = 0.1829$, $R_{pw} = 0.2805$) (Figure S1 in Supporting Information).[26] From this result, the trend of the *a* axis distance was found to be **1** < **4** < **5** < **3** ≈ **2**, and hence, the interlayer distance trend is expected to be **1** < **4** < **5** < **3** ≈ **2**. Compounds **1** and **5** crystallize with three *p*-xylene molecules per unit, and **2** and **4** crystallize with one *p*-xylene molecule and highly disordered *p*-xylene and/or CH_2Cl_2 molecules. Typically, one *p*-xylene molecule stacks with the $TCNQR_x$ moiety, forming a $\pi-\pi$ stacking column with a [···($TCNQR_x$)···(*p*-xylene)···] repeat, such that there is no direct contact between layers. The remaining solvent molecules are in the hexagonal cavity of 2-D network.

Structural Characterization of 1-Rh−5-Rh. Except for **2-Rh** and **3-Rh** (which, like **3**, are severely twinned), crystals of the dirhodium series were characterized by single-crystal X-ray crystallography. The cell parameters of **2-Rh** and **3-Rh** were checked by XRPD (Figure S2 in Supporting Information) with the LeBail method:[26] $a = 19.991(3)$ Å, $b = 20.223(3)$ Å, $c = 8.6537(10)$ Å, $\beta = 100.678(11)°$ with *C*2/*m* ($R_p = 0.2444$, $R_{pw} = 0.3850$) for **2-Rh** and $a = 19.754(2)$ Å, $b = 20.115(2)$ Å, $c = 8.6436(9)$ Å, $\beta = 100.256(8)°$ with *C*2/*m* ($R_p = 0.2415$, $R_{pw} = 0.3526$) for **3-Rh**. The Rh_2 compounds are very similar to the corresponding Ru_2 series, but only **5-Rh** crystallizes in the monoclinic $P2_1/c$ space group with an inversion center at the midpoint of the $TCNQF_4$ ligand ($Z = 2$) (Table 1). Therefore, **5-Rh** has two kinds of Rh−$N_{N\equiv C}$ bonds. Thermal ellipsoid drawings of the basic structures of **1-Rh**, **4-Rh**, and **5-Rh** and packing diagrams for **5-Rh** are depicted in Figure S3 and S4 in Supporting Information, respectively. The Rh−Rh bond lengths of **1-Rh**, **4-Rh**, and **5-Rh** are 2.4080(3), 2.4057(8), and 2.4223(8) Å, respectively, similar to that of $[Rh_2^{II,II}(O_2CCF_3)_4(L)]$ (2.391−2.408 Å for L = THF;[27] 2.391−2.426 Å for L = DMSO)[28] but characteristically much longer than those of the Ru series (vide infra), which is attributed to the nature of the M−M bond electronic configuration. The metal−metal bond is, formally, a single one for $[Rh_2^{II,II}]$ (singlet ground state with $\sigma^2(2\pi)^4\delta^2\delta^{*2}(2\pi^*)^4$), a double bond for $[Ru_2^{II,II}]$ (triplet ground state with $\sigma^2(2\pi)^4\delta^2\delta^{*2}(2\pi^*)^2$), and a double and half for $[Ru_2^{II,III}]$ (quartet ground state with $\sigma^2(2\pi)^4\delta^2(\delta^*2\pi^*)^3$).[29] The Rh−$N_{N\equiv C}$ bond lengths of **1-Rh**, **4-Rh**, and **5-Rh** are 2.184(2), 2.187(6), and 2.194(5) (Rh(1)−N(1)) and 2.203(5) (Rh(2)−N(2)) Å, respectively, which are slightly shorter than the corresponding distances for the Ru−$N_{N\equiv C}$ distances.

(27) Cotton, F. A.; Dikarev, E. V.; Stiriba, S.-E. *Inorg. Chem.* **1999**, *38*, 4877.

(28) Cotton, F. A.; Dikarev, E. V.; Petrukhina, M. A.; Stiriba, S.-E. *Inorg. Chem.* **2000**, *39*, 1748.

(29) (a) Cotton, F. A.; Walton, R. A. *Multiple Bonds Between Metal Atoms*, 2nd ed.; Oxford University Press: Oxford, 1993. (b) *Multiple Bonds Between Metal Atoms*, 3rd ed.; Cotton, F. A., Murillo, C. A., Walton, R. A., Eds.; Springer Science and Business Media, Inc.: New York, 2005.

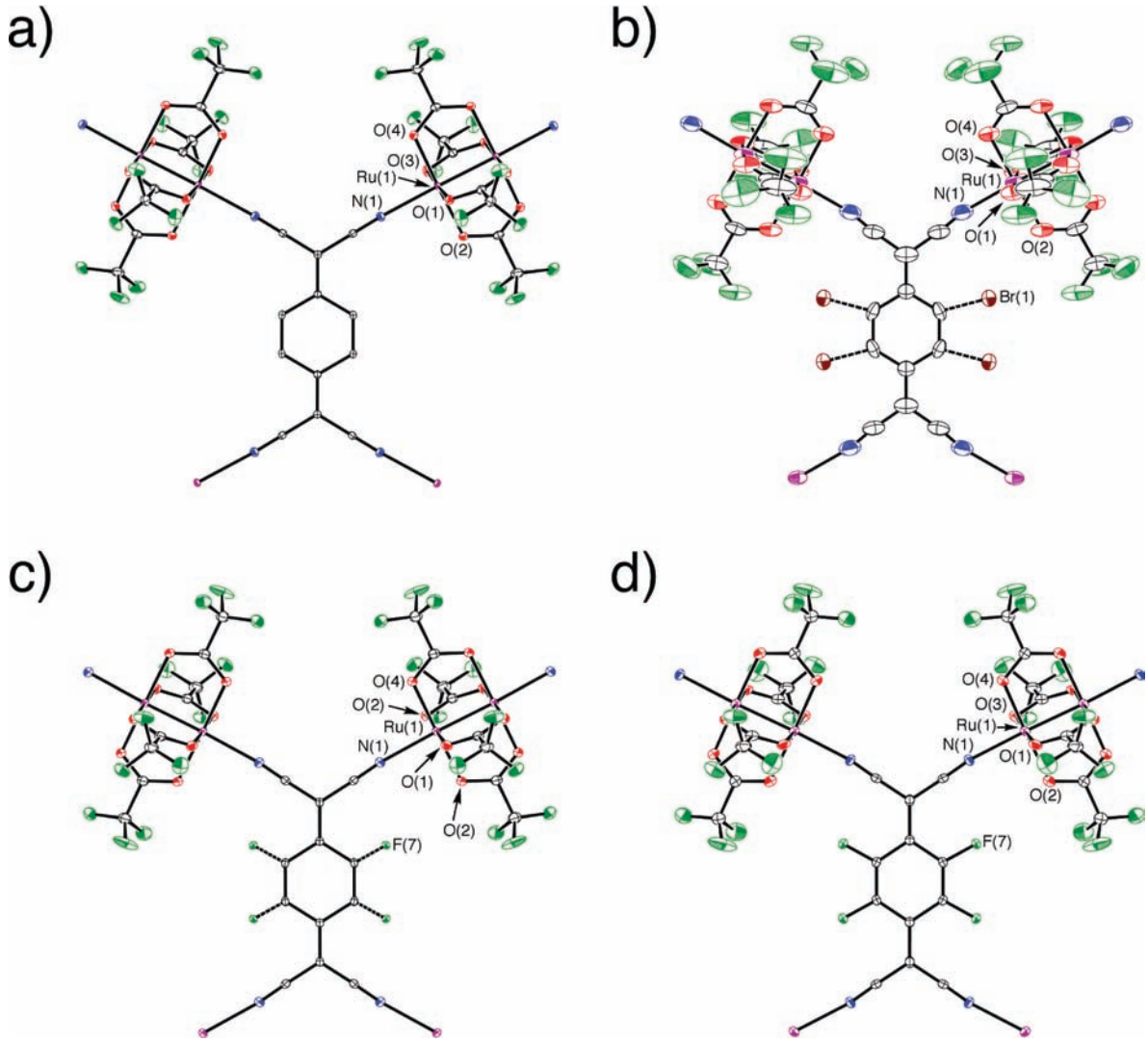

Figure 1. Thermal ellipsoid drawings of formula unit of **1** (a), **2** (b), **4** (c), and **5** (d) with atomic labeling for selected atoms (30% probability ellipsoids), where the dotted bonds in **2** (b) and **4** (c) represent disordered atoms. Hydrogen atoms and solvent molecules were omitted for the sake of clarity.

Effect of Charge Transfer on Structures. The Ru−Ru bond lengths of **1**, **2**, **4**, and **5** are 2.2921(2), 2.2854(13), 2.2937(3), and 2.3040(6) Å, respectively, which are very similar to each other and to that of the starting material, $[Ru_2^{II,II}(O_2CCF_3)_4(THF)_2]$ (2.276(3) Å).[15] The Ru−O_{eq} (O_{eq} = carboxylate oxygen) average bond lengths are 2.0712(40), 2.0588(78), 2.0717(42), and 2.0592(74) Å, respectively. In general, the Ru−O_{eq} bond lengths in the series of paddlewheel $[Ru_2(O_2CR)_4]^{n+}$ complexes are affected by the oxidation state of $[Ru_2]$ center and are approximately 2.07 Å for $[Ru_2^{II,II}]$ and 2.02 Å for $[Ru_2^{II,III}]^+$ complexes; although the difference between them is rather small, there is a clear trend.[29] In support of this point, there is the fact that the distances in $[Ru_2^{II,II}(O_2CCF_3)_4(THF)_2]$[15] and $[Ru_2^{II,III}(O_2CCF_3)_4](O_2CCF_3)$[16] are 2.073 and 2.024 Å, respectively. The Ru−O_{eq} bond distances of **2** and **5** are intermediate between $[Ru_2^{II,II}]$ and $[Ru_2^{II,III}]^+$ (but since **2** has relative large esd errors in bond lengths, this estimation is not particularly accurate), whereas those of **1** and **4** are close to the case of $[Ru_2^{II,II}]$.

It is well-known that the C−C bond lengths in TCNQ reflect the oxidation state of TCNQ because the TCNQ ring reverts from a quinonoid form to a benzenoid form with increasing charge.[30] The charge of TCNQ can be estimated by Kistenmacher relationship $\rho = A[c/(b + d)] + B$,[31] where $b-d$ are the distances of $TCNQR_x$ defined in the figure of Table 2 and A and B are parameters determined by assuming a complete neutral and a fully ionized (i.e., $1e^-$-reduced) form of $TCNQR_x$ such as $TCNQ^0$ ($\rho = 0$)[32]/RbTCNQ[33] ($\rho = -1$) and $TCNQF_4^0$ ($\rho = 0$)[34]/(n-Bu_4N)$TCNQF_4$[35] ($\rho = -1$), and $A_H = -41.667$ and $B_H = 19.833$ for TCNQ and $A_{F4} = -46.729$ and $B_{F4} = 22.308$ for $TCNQF_4$. The relevant bond distances in the $TCNQR_x$ moiety are listed in Table 2. Unfortunately, there are no suitable references for neutral and 1-e^--reduced forms for $TCNQF_2$ and $TCNQBr_2$ in order to assess the A and B parameters. Nevertheless, the calculation based on the original TCNQ set can be

(30) Flandrois, S.; Chasseau, D. *Acta Crystallogr., Sect. B* **1977**, *33*, 2744.
(31) Kistenmacher, T. J.; Emge, T. J.; Bloch, A. N.; Cowan, D. O. *Acta Crystallogr., Sect. B* **1982**, *38*, 1193.
(32) Long, R. E.; Sparks, R. A.; Trueblood, K. N. *Acta Crystallogr.* **1965**, 18.
(33) Hoekstra, A.; Spoelder, T.; Vos, A. *Acta Crystallogr. Sect. B* **1972**, *28*, 14.
(34) Emge, T. J.; Maxfield, M.; Cowan, D. O.; Kistenmacher, T. J. *Mol. Cryst. Liq. Cryst.* **1981**, *65*, 161.
(35) O'Kane, S. A.; Clérac, R.; Zhao, H.; Ouyang, X.; Galán-Mascarós, J. R.; Heintz, R.; Dunbar, K. R. *J. Solid State Chem.* **2000**, *152*, 159.

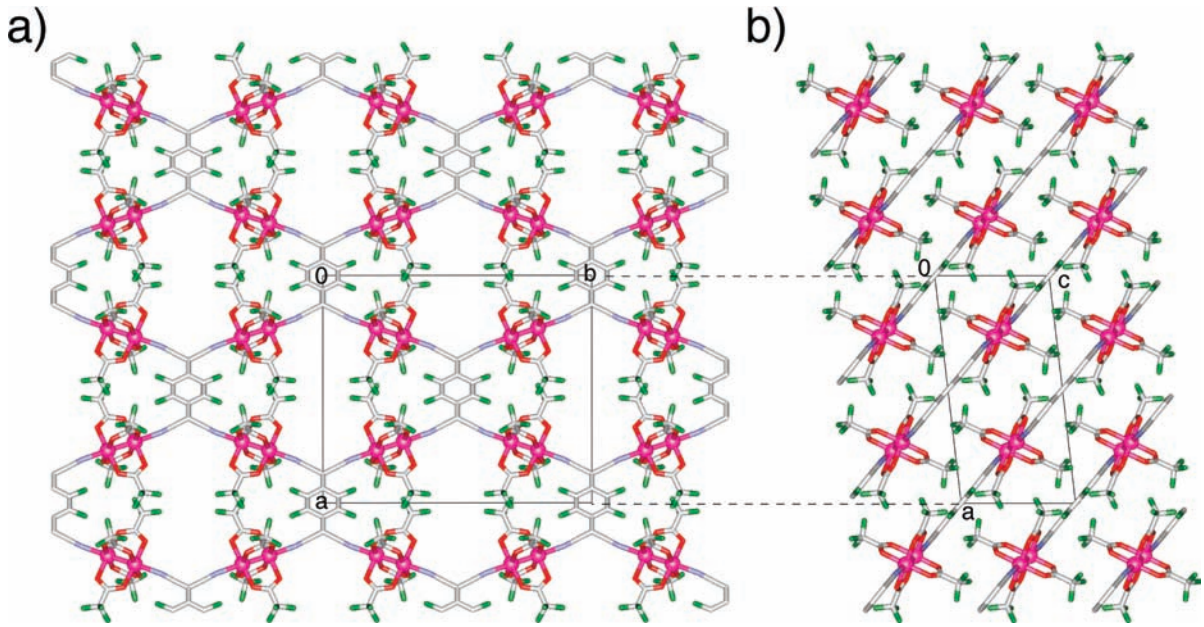

Figure 2. Packing diagrams of **5** projected along (a) the *c* axis and (b) the *b* axis. The solvent molecules (three *p*-xylene molecules) were omitted for the sake of clarity.

Table 2. Bond Distances in the $TCNQR_x$ Moiety and Degree of Charge Transfer (ρ) Estimated from the Kistenmacher Relationship[a]

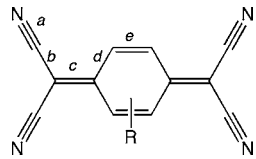

	assumed charge	*a*	*b*	*c*	*d*	*e*	*b* + *d*	*c*/(*b* + *d*)	ρ[a]
TCNQ[c]	0	1.140(1)	1.441(4)	1.374(3)	1.448(4)	1.346(3)	2.889	0.476	0
RbTCNQ[d]	−1	1.153(7)	1.416(8)	1.420(1)	1.423(3)	1.373(1)	2.839	0.5	−1
$TCNQF_4$[e]	0		1.437	1.372	1.437		2.874	0.477	0
(*n*-Bu_4N)$TCNQF_4$[f]	−1		1.426	1.418	1.417		2.843	0.499	−1
1-Rh·3(toluene)[g]	0	1.131(6)	1.436(5)	1.409(9)	1.432(5)	1.358(8)	2.868	0.491	−0.63
1-Rh·3(*p*-xylene)	0	1.139(4)	1.428(4)	1.393(6)	1.440(3)	1.351(4)	2.868	0.486	−0.42
4-Rh·2.7(*p*-xylene)·0.8CH_2Cl_2	0	1.140(9)	1.431(9)	1.384(14)	1.429(8)	1.352(10)	2.860	0.484	−0.33
5-Rh·3(*p*-xylene)	0	1.140(8)	1.432(9)	1.379(10)	1.452(9)	1.340(9)	2.8895	0.477	−0.042
		1.139(9)	1.442(9)		1.453(9)				(0)[b]
		av 1.1395	av 1.437		av 1.4525				
1·3(toluene)[g]		1.132(4)	1.431(4)	1.393(6)	1.435(4)	1.349(6)	2.866	0.486	−0.42
1·3(*p*-xylene)		1.140(3)	1.433(3)	1.393(5)	1.444(3)	1.359(3)	2.877	0.484	−0.33
2·*p*-xylene·2CH_2Cl_2		1.14(2)	1.457(18)	1.37(2)	1.421(12)	1.373(14)	2.878	0.476	0
4·2.3(*p*-xylene)·1.4CH_2Cl_2		1.132(4)	1.438(4)	1.381(7)	1.443(4)	1.353(5)	2.881	0.479	−0.13
5·3(*p*-xylene)[h]		1.126(7)	1.431(7)	1.419(11)	1.416(6)	1.351(7)	2.847	0.498	−0.92 (−0.96)[b]

[a] $\rho = A_H[c/(b + d)] + B_H$ with $A_H = -41.667$ and $B_H = 19.833$. [b] The ρ value estimated using $A_{F4} = -46.729$ and $B_{F4} = 22.308$ (see text). [c] Reference 32. [d] Reference 33. [e] Reference 34. [f] Reference 35. [g] Reference 24. [h] Reference 25.

viewed as a qualitative approximation for the $TCNQR_x$ series and even for $TCNQF_4$ as indicated by the similarity of the [*c*/(*b* + *d*)] values obtained from $TCNQ^0$/$TCNQF_4^0$ and RbTCNQ/(*n*-Bu_4N)$TCNQF_4$ (Table 2). Therefore, all compounds were subjected to calculations based on the equation for the original TCNQ set (Table 2). The virtual charge transfer from [Ru_2] unit to the $TCNQR_x$ molecule seems to be absent in **1**·3(*p*-xylene) ($\rho = -0.33$), **2** ($\rho \approx 0$), and **4** ($\rho = -0.13$), but the $TCNQF_4$ moiety in **5** is 1-e^--reduced ($\rho = -0.92$; $\rho = -0.96$ evaluated using A_{F4} and B_{F4}). All of the Rh compounds, including **5-Rh**, are expected to be neutral without virtual charge transfer to $TCNQR_x^{\bullet -}$, although π-back-donations of $[Rh_2^{II,II}] \rightarrow TCNQR_x$ can be stronger than in the diruthenium series with values as high as −0.63 of ρ being observed (Table 2). From these results, at least for **5**, it is concluded that a full 1-e^- charge transfer from two $[Ru_2^{II,II}(O_2CCF_3)_4]$ units to one $TCNQF_4$ has occurred, viz., it is formally [{$Ru_2^{4.5+}$}-($TCNQF_4^{\bullet -}$)-{$Ru_2^{4.5+}$}]. Additional information about the oxidation state of $TCNQR_x$ was obtained by infrared spectroscopy.

Determination of Oxidation State by Infrared Spectroscopy. IR spectra were measured on KBr pellets of **1**−**5** and **1-Rh**−**5-Rh** at room temperature. The vibrational modes of ν(C≡N) and ν(C=C) for $TCNQR_x$ are characteristic of the oxidation state of $TCNQR_x$. The ν(C≡N) mode for all Ru_2 compounds (**1**−**5**) was observed as multiplets: the values are 2238, 2198, and 2134 cm^{-1} for **1**, 2216w, 2198, 2158, and 2123 cm^{-1} for **2**, 2223w, 2200, 2161, and 2126 cm^{-1} for **3**, 2231w, 2207, and 2141 cm^{-1} for **4**, and 2217 and 2182 cm^{-1} for **5** (Figure S5 in Supporting Information). Most of them are shifted to lower energies from the b_{1u} and b_{2u} modes of the neutral

$TCNQR_x^0$ molecules (2222 cm^{-1} for $TCNQ^0$,[36] 2218 and 2193 cm^{-1} for $TCNQBr_2^0$, 2225 and 2208 cm^{-1} for $TCNQCl_2^0$, 2223 and 2204 cm^{-1} for $TCNQF_2^0$, 2226 and 2213 cm^{-1} for $TCNQF_4^0$[37] (Figure S5 in Supporting Information)), with only the highest ν(C≡N) frequency band observed for **1** and **4** being observed at a higher energy than of $TCNQR_x^0$. All of the compounds in the dirhodium series are similar to **1** and **4**; both lower- and higher- energy shifts are observed; the values are 2245, 2226, 2196 cm^{-1} for **1-Rh**, 2228 and 2195 cm^{-1} for **2-Rh**, 2233 and 2198 cm^{-1} for **3-Rh**, 2239 and 2200 cm^{-1} for **4-Rh**, and 2246, 2219, and 2166 cm^{-1} for **5-Rh** (Figure S5 in Supporting Information). Since the ν(C≡N) mode is affected by the nature of the metal bonding interaction as well as the redox state, we cannot simply compare these energy shifts with the degree of oxidation, but the lower energy absorptions indicative of back-donating interactions even with the Rh series and compound **1** with TCNQ which has the lowest electron affinity among the $TCNQR_x$ series. Qualitatively, the presence of virtual charge transfer is taken to be the case when all of the ν(C≡N) modes shift to lower energies, as is the case for **5**.

The ν(C═C) stretch in $TCNQR_x$ is also an important indicator of the degree of oxidation. Figure 3 shows IR spectra of $TCNQR_x^0$, $LiTCNQR_x$, **1**−**5**, and **Rh-1**−**Rh-5** in the frequency range of 1600−1400 cm^{-1} (1650−1400 cm^{-1} for **5** and **5-Rh**). A comparison of the spectra between the Ru series and Rh series reveals that there are three distinctive sets of patterns: [**1** and **4**], [**2** and **3**], and [**5**]. The first set [**1** and **4**] exhibits characteristic ν(C═C) modes for $TCNQR_x^0$ without any signature for $TCNQR_x^{\bullet -}$ (a and b in Figure 3). The respective Rh compounds are basically the same. The second set [**2** and **3**] reveals modes characteristic of $TCNQR_x^{\bullet -}$ even in **2-Rh** and **3-Rh** (c and d in Figure 3). Finally, the third set [**5**] is similar to the second set in that there are ν(C═C) modes typical for $TCNQR_x^{\bullet -}$, but it is noted that the **5-Rh** compound has absorptions in the range of $TCNQR_x^0$ (e in Figure 3). Thus, the shift of the ν(C═C) mode varies not only by the degree of charge transfer (including π-back-donation independent of formal redox state) but is also dependent on the substituents R_x of $TCNQR_x$. Therefore, it is not accurate to estimate the degree of oxidation by simply inspecting the diruthenium series; a meaningful assessment can only be made by a comparison to the dirhodium series. We point out at this stage that Horiuchi et al. have proposed that the oxidation state of TCNQ derivatives is linearly correlated with the degree of ν(C═C) shift and employed the empirical equation $\rho = -(\omega^{obs} - \omega^0/\omega^1 - \omega^0)$ to estimate the oxidation degree (ρ) of target compounds, where ω^{obs}, ω^0, and ω^1 are the ν(C═C) mode frequency of the target compound, $TCNQR_x^0$, and $TCNQR_x^{\bullet -}$, respectively.[20] Although this equation has been used for nonbonded species, in principle, the same procedure may be applied to directly bonded TCNQ series for comparison sake. The ν(C═C) mode (b_{1u} and b_{2u}) of neutral/1e$^-$-reduced forms of $TCNQR_x$ and related modes observed for all compounds were determined as listed in Table 3 from the IR data in Figure 3, and the b_{2u} frequency was used to estimate ρ values. The value for $TCNQR_x^{\bullet -}$ was taken from a spectrum of $LiTCNQR_x$. In the Ru series, the ρ values for **2**, **3**, and **5** suggest a full charge transfer to $TCNQR_x^{\bullet -}$, whereas those for **1** and **4** indicate a neutral form. However, an assessment of **2-Rh** and **3-Rh** also derive the same degree of ρ as **2** and **3** despite the fact that no virtual charge transfer could

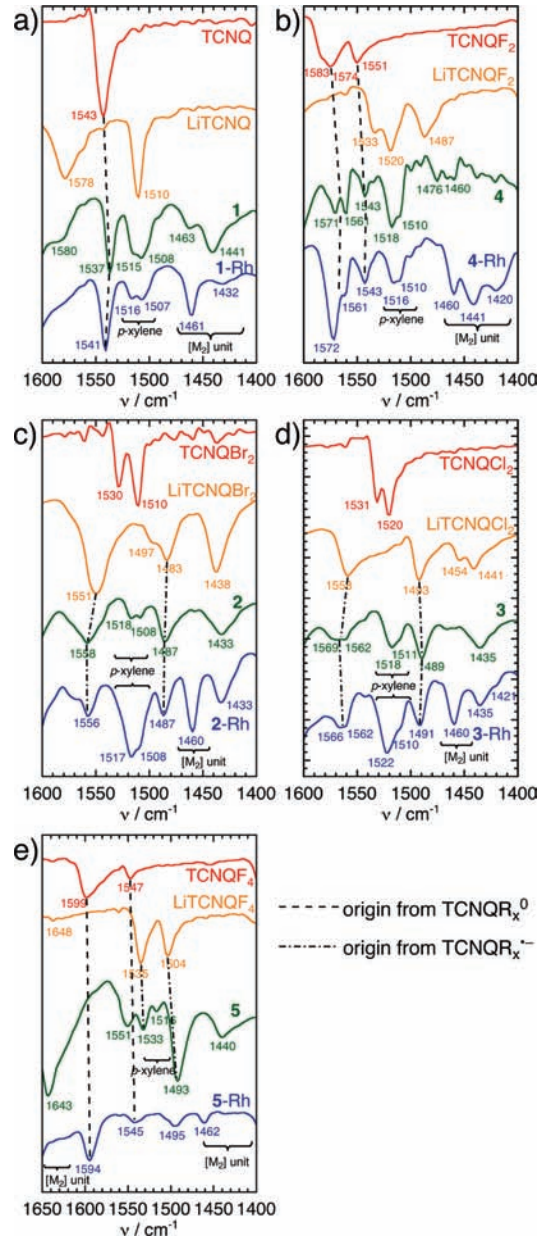

Figure 3. Infrared spectra in the range of 1400−1600 cm^{-1} (or 1650 cm^{-1}) of $TCNQR_x^0$, $LiTCNQR_x$, **1**−**5**, and **1-Rh**−**5-Rh** measured on KBr pellets at room temperature, where panels a−e represent sets of [**1**], [**4**], [**2**], [**3**], and [**5**], respectively.

be anticipated. Hence, in order to estimate the degree of virtual oxidation ρ_v in the Ru series, the value of $\rho_v = (\rho_{Ru} - \rho_{Rh})$ is used as listed in Table 3. These values indicate that only **5** has undergone a full charge transfer of $[Ru_2^{II,II}] \rightarrow TCNQF_4$ to form $TCNQF_4^{\bullet -}$ and that the TCNQ units in the other diruthenium compounds are close to neutral at room temperature.

In summary, the IR data including the comparison between the Ru and Rh series have provided useful information on the static oxidation state of $TCNQR_x$ and are consistent with the structural characteristics.

Magnetic Properties. The temperature dependence of the dc susceptibility data for **1**−**5** was measured at 0.1 or 1 T in the temperature range of 1.8−300 K. Figure 4 shows the χT product and χ^{-1} plots for **1**−**5** as a function of temperature. The χT values at 300 K of **1**−**5** are 1.86, 2.01, 1.94, 1.87, and 2.02 $cm^3 \cdot K \cdot mol^{-1}$, respectively, which is nearly twice the value for

(36) Meneghetti, M.; Girlando, A.; Pecile, C. *J. Chem. Phys.* **1985**, *83*, 3134.
(37) Meneghetti, M.; Pecile, C. *J. Chem. Phys.* **1986**, *84*, 4149.

Table 3. Data for C=C Stretching Modes (cm^{-1}) in the IR Spectra of $TCNQR_x$, $LiTCNQR_x$, and the Present Compounds and Degree of Charge Transfer[a] (ρ)

Compound	$\nu_{C=C}$ of $TCNQR_x$ (ω^0)/cm^{-1}	$\nu_{C=C}$ of $LiTCNQR_x$ (ω^1)/cm^{-1}	$\nu_{C=C}$ of comp.[b] (ω^{obs})/cm^{-1}	ρ^c	ρ_v[e]
1·3(*p*-xylene) (R_x = H)	1543 (b_{1u} + b_{2u})	1510 (b_{2u}); 1578 (b_{1u})	1537 ω^0; 1580w ω^1[d]	−0.18	−0.12
1-Rh·3(*p*-xylene) (R_x = H)			1541 ω^0	−0.06	
2·*p*-xylene·$2CH_2Cl_2$ (R_x = Br_2)	1510 (b_{2u}); 1530 (b_{1u})	1483 (b_{2u}); 1497w (b_{2u}); 1551 (b_{1u})	1487 ω^1; 1558 ω^1	−0.85	0
2-Rh (R_x = Br_2)			1487 ω^1; 1556 ω^1	−0.85	
3 (R_x = Cl_2)	1520 (b_{2u}); 1531 (b_{1u})	1493 (b_{2u}); 1558 (b_{1u})	1489 ω^1; 1562 ω^1	−1.15	−0.08
3-Rh (R_x = Cl_2)			1491 ω^1; 1562 ω^1	−1.07	
4·2.3(*p*-xylene)·$1.4CH_2Cl_2$ (R_x = F_2)	1551 (b_{2u}); 1574 (b_{1u}); 1583w (b_{1u})	1487 (b_{2u}); 1520 (b_{1u}); 1533 (b_{1u})	1543 ω^0; 1561 ω^0; 1571 ω^0	−0.26	0
4-Rh·2.7(*p*-xylene)·$0.8CH_2Cl_2$ (R_x = F_2)			1543 ω^0; 1561 ω^0; 1572 ω^0	−0.26	
5·3(*p*-xylene) (R_x = F_4)	1547 (b_{2u}); 1599 (b_{1u})	1504 (b_{2u}); 1535 (b_{1u})	1493 ω^1; 1533 ω^1	−1.26	−1.21
5-Rh·3(*p*-xylene) (R_x = F_4)			(1495 ω^1)[d]; 1545 ω^0; 1594 ω^0	−0.05	

[a] Estimated from the relation of $\rho = -(\omega^{obs} - \omega^0/\omega^1 - \omega^0)$ based on the underlined data. [b] ω^0 and ω^1 stand for the assignment of the origin of mode. [c] Individual ρ value estimated based on the underlined values. [d] Uncertain assignment. [e] $\rho_v = \rho_{Ru} - \rho_{Rh}$.

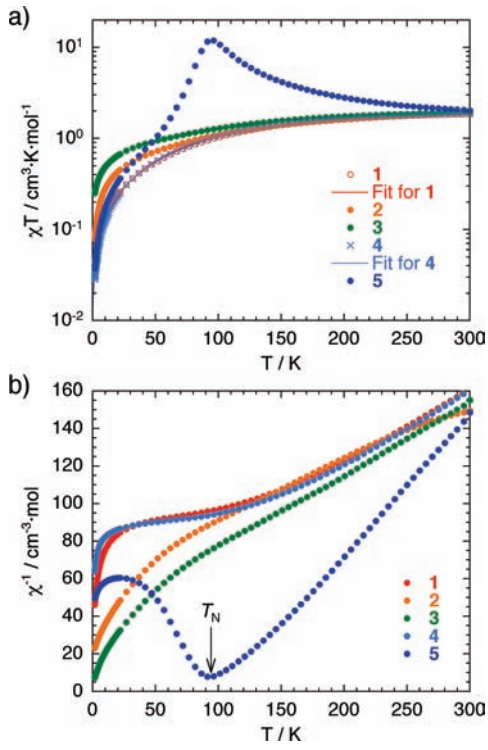

Figure 4. χT (a) and χ^{-1} (b) vs T plots for **1**−**5**. In (a), the solid red and pale blue curves for **1** and **4**, respectively, represent simulation curves to an S = 1 paramagnetic model taking into account zero-field splitting, temperature-independent paramagnetism, and a contribution of a S = 3/2 species ($[Ru_2^{II,III}]$) as an impurity (see text).

isolated $[Ru_2^{II,II}]$ complexes with S = 1 (0.9−1.2 $cm^3 \cdot K \cdot mol^{-1}$ per $[Ru_2^{II,II}]$) compared to that of isolated $[Ru_2^{II,III}]^+$ complexes with S = 3/2 (1.8−2.2 $cm^3 \cdot K \cdot mol^{-1}$ per $[Ru_2^{II,III}]^+$). Except for **5**, the χT values for **1**−**4** decrease continuously as the temperature is lowered to reach 0.04, 0.08, 0.25, and 0.03 $cm^3 \cdot K \cdot mol^{-1}$, respectively, at 1.8 K. However, as shown in Figure 4b, the χ^{-1} vs T behavior for **1** and **4**, which exhibit a near-plateau region at temperatures of 30−100 K with an inflection point at around 100 K, is reminiscent of isolated $[Ru_2^{II,II}]$ complexes (S = 1).[15] Given this resemblance, the χ and χT vs T plots for **1** and **4** were simulated using an S = 1 Curie paramagnetic model taking into account anisotropy due to second-order Zeeman splitting of the ground term (D, zero-field splitting parameter), temperature-independent paramagnetism (TIP), and an impurity (ρ) as a $[Ru_2^{II,III}]^+$ species with S = 3/2.[38] In addition, the intermolecular interaction (zJ) was introduced in the frame of the mean-field approximation. The parameters obtained from the fitting are accord with a completely isolated typical $[Ru_2^{II,II}]$ unit with zJ = 0: g = 2.0 (fixed), D = 271 cm^{-1}, TIP = 44 × 10^{-6} $cm^3 \cdot mol^{-1}$, and ρ = 0.0079 for **1** and g = 2.0 (fixed), D = 257 cm^{-1}, TIP = 66 × 10^{-6} $cm^3 \cdot mol^{-1}$, and ρ = 0.0064 for **4**. These results are consistent with what was concluded for these compounds on the basis of the structural and IR studies, namely, that **1** and **4** exist in the resonance form [{Ru_2^{4+}}-($TCNQR_x^0$)-{Ru_2^{4+}}] without charge transfer between the $[Ru_2^{II,II}]$ and $TCNQR_x$ over the temperature range studied.

Compounds **2** and **3** exhibit χ values that increase continuously with decreasing temperature, which is clearly different from the data for **1** and **4**. These differences in **2** and **3** as compared to **1** and **4** are more easily discerned from their χ^{-1} vs T plots (Figure 4b), in which the divergence from those for **1** and **4** is found below ∼120 K. These data are in accordance with the high-temperature behavior of **2** and **3** being defined by isolated $[Ru_2^{II,II}]$ units with intralayer, interunit interactions becoming evident at lower temperatures. These results can be considered in terms of a scenario often used for organic semiconductors:[39] Even if the virtual oxidation state of $TCNQBr_2$ or $TCNQCl_2$ is assigned to be neutral (quasi-static neutral state as well as **1** and **4**), thermally activated charge transfers can occur. Such charge transfers, in general, do not contribute magnetically but can lead to charge localization to produces radical spins on some of $TCNQR_x$ moieties originating most likely from structural fluctuations and the presence of defects caused, for example, by disordered interstitial solvent molecules. These defects are important at sufficiently low temperatures and can mediate short-range magnetic order. This hypothesis is also supported by the fact that **2** and **3** exhibit higher conductivity than **1** and **4** even as semiconductors (vide infra).

The most dramatic change in magnetism from the behavior of **1** with isolated diruthenium paramagnetic units is exhibited by **5**, which demonstrates a full 1-e^- charge transfer from the combined $[Ru_2^{II,II}]$ units to $TCNQF_4$. The χT product increases below 300 K to reach a maximum of 11.9 $cm^3 \cdot K \cdot mol^{-1}$ at 96 K (Figure 4a) and then suddenly drops to ∼1 $cm^3 \cdot K \cdot mol^{-1}$ (at 60 K). Finally there is a gradual decrease to 0.037 $cm^3 \cdot K \cdot mol^{-1}$ at 1.8 K. The increase of χT at high temperatures is attributed to strong coupling between spins in a layer mediated by the $TCNQF_4^{\bullet -}$ radical. The Weiss constant (θ) estimated from χ^{-1} in the high temperature range (160−300 K) is 104 K. The peak of χT corresponds to that of χ at 93 K (at 1 kOe) (Figure 4b),

(38) Miyasaka, H.; Campos-Fernández, C. S.; Clérac, R.; Dunbar, K. *J. Chem. Soc., Dalton Trans.* **2001**, 858.
(39) Hiraga, H.; Miyasaka, H.; Clérac, R.; Fourmigué, M.; Yamashita, M. *Inorg. Chem.* **2009**, *48*, 2887.

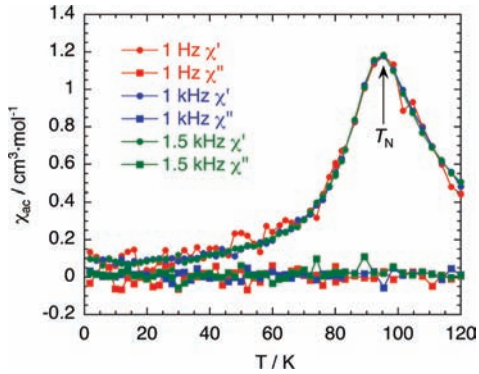

Figure 5. Temperature dependence of ac susceptibilities measured at zero dc field and a 3 Oe ac oscillation field where the peak temperature (95 K) is the Néel temperature (T_N).

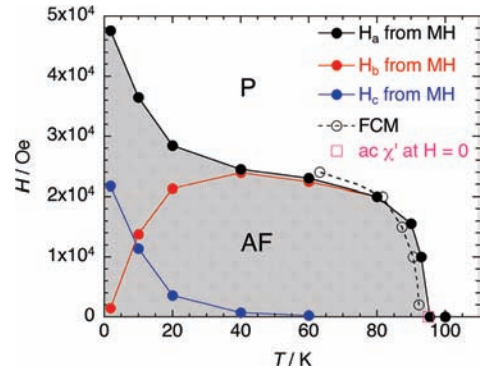

Figure 7. Temperature dependence of critical fields, H_a, H_b, and H_c, and field dependence of T_N in **5**, showing the phase diagram separating a paramagnetic (P) phase and an antiferromagnetic (AF) phase.

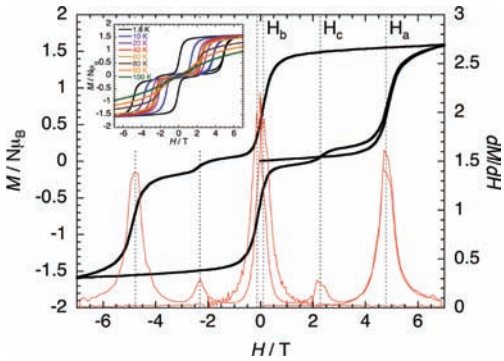

Figure 6. Field dependence of the magnetization (M) and dM/dH at 1.8 K of **5**. Inset: temperature dependence of MH curve measured in the range of 1.8−100 K.

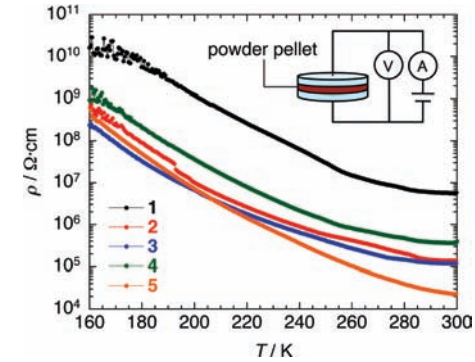

Figure 8. Temperature dependence of the resistivity (ρ) measured on pressed pellet powder samples of **1**−**5**.

which indicates the occurrence of antiferromagnetic long-range order attributed to interlayer antiferromagnetic interactions. The fact that the in-phase ac susceptibility signal (χ') measured at zero dc field follows the temperature dependent feature of the dc susceptibility without an out-of-phase ac susceptibility (χ'') anomaly even at around the peak of χ' at ca. 95 K (= T_N) (Figure 5) supports this hypothesis. Nevertheless, field dependence of the magnetization of **5** indicates that the compound is not a general antiferromagnet. At 1.8 K, the initial sweep from 0 to 7 T shows a sigmoidal increase of the magnetization with a critical field of 4.74 T, indicating a spin flip from an antiferromagnetic phase (AF) to a paramagnetic phase (P), i.e., a metamagnetic transition. Moreover, during the forward and reverse sweeps between 7 and −7 T, three kinds of steps are observed at ±0.20 (H_b), ±2.38 (H_c), and ±4.74 (H_a) T with a large butterfly type hysteresis being evident (Figure 6). The presence of three steps indicates the existence of a canted spin phase (CS): P→CS, CS(+)→(AF)→CS(−), and CS→P, respectively. Upon increasing the temperature, the hysteresis and spin flip at H_c disappear relative to one another at ∼60 K, and the metamagnetic spin flip (AF→P or CS→P at H_a) disappears at ∼95 K, consistent with the peak temperature in χT and χ (Figure 7). Thus, the metamagnetic-like nature with a large hysteresis in **5**, i.e., indicating field-induced magnetic behavior, likely originates from interlayer antiferromagnetic interactions coupled with strong anisotropy arising from the [Ru_2] units.[40]

Thus, the magnetic behavior observed in the present series is strongly associated with charge transfer from [$Ru_2^{II,II}$] units to the $TCNQR_x$ bridges.

Dc Electrical Resistivity of 1−5. Dc electrical resistivity on pressed pellet samples of **1**−**5** and **1-Rh**−**5-Rh** was measured over the temperature range of 160−300 K. Pellets of size d = 3 mm ϕ and $l \approx 0.3$ mm were sandwiched between two isometric brass plates and platinum probe wires were attached. Unfortunately, attempts to make measurements on single crystals were not successful because of the extreme fragility of crystals in addition to their small size. Figure 8 depicts the temperature dependence of the resistivity (ρ) on pellet samples of **1**−**5**. The resistivity for **1**− **5** is 5.8 × 10^6 Ω·cm (σ = 1.7 × 10^{-7} S·cm^{-1}), 1.4 × 10^5 Ω·cm (σ = 7.1 × 10^{-6} S·cm^{-1}), 1.2 × 10^5 Ω·cm (σ = 8.3 × 10^{-6} S·cm^{-1}), 4 × 10^5 Ω·cm (σ = 2.5 × 10^{-6} S·cm^{-1}), and 2.3 × 10^4 Ω·cm (σ = 4.4 × 10^{-5} S·cm^{-1}) at room temperature, respectively, and increases with a decrease in temperature, indicating semiconductor behavior. The activation energy (E_a) is roughly estimated as 308, 265, 240, 269, and 303 meV for **1**− **5**, respectively. Despite the rough measurements using powder pellets, a comparison of their room temperature resistivity reveals that the electronic properties of **1**−**5** can be classified into three groups: group I, **1**; group II, **2**−**4** with an order of **4** < **2** ≈ **3** in their conductivity; and group III, **5**. From structural and IR studies, **1**−**4** were characterized as being in quasi-neutral forms with no virtual charge transfer from [$Ru_2^{II,II}$] to $TCNQR_x$. Nevertheless, the resistivity of **2**−**4** is clearly lower than that of **1**, which interestingly follows the order of electron affinity of $TCNQR_x$ ($H_4 \ll F_2 < Br_2 \sim Cl_2$). This trend of resistivity represents the mobility of [$Ru_2^{II,II}$]→$TCNQR_x$ activated thermally and/or by an electric field and follows the order of electron affinity of $TCNQR_x$. The compounds in the Rh series are insulators with $\rho_{rt} > 10^7$ Ω·cm even on single crystals.

(40) Kurmoo, M. *Chem. Soc. Rev.* **2009**, *38*, 1353, and references therein.

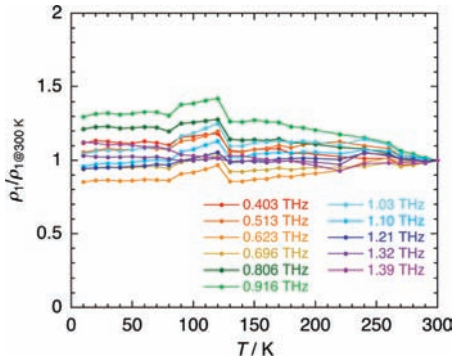

Figure 9. Normalized resistivity (ρ_1) of **1** as a function of temperature measured at several frequencies by THz-TDS.

Terahertz Time-Domain Spectroscopy for 1 and 5. The correlation between the local ordered spins produced by interunit charge transfers as observed in **5** and electron transport properties is one of the main topics of this collective study. As mentioned above, however, the measurements of single-crystal dc electrical resistivity by making direct electrical contacts using thin probe wires with conductive pastes were unsuccessful. Therefore, terahertz time-domain spectroscopy (THz-TDS), which is a powerful tool to obtain noncontact and nondestructive evaluation of the intrinsic electronic properties of a compound,[41] was undertaken using polycrystalline pellets with a thickness (d) of 0.2 mm of **1** and **5** attached on a cellophane tape with a thickness of 0.05 mm in the temperature range of 6−300 K. The THz-TDS technique records a THz wave profile of the transmission amplitude of the target sample as a function of time (Figure S6 in Supporting Information), which directly yields both real and imaginary parts of complex electronic conductivity ($\sigma^* = \sigma_1 + i\sigma_2$) and dielectric permittivity ($\varepsilon^* = \varepsilon_1 + i\varepsilon_2 = \varepsilon_1 + i4\pi\sigma_1/\omega$) without the Kramers−Kronig transformation, where $\omega = 2\pi\nu$ is the angular frequency.[42] Experimental details are noted in the experimental section, but it should be mentioned here that the magnetic permeability (μ_1) in the frequency and temperature range of our experiments needed to estimate ε^* and σ^* from the raw data was assumed to be constant at $\mu_1 = 1$ (vide infra). Figures 9 and 10 show the temperature dependence of the normalized resistivity ($\rho_1 = 1/\sigma_1$) and dielectric constant (ε_1) for **1** and **5**, respectively, at several frequencies ($\nu = 0.4-1.7$ THz). In **1** (Figure 9), both parameters exhibit no characteristic variation throughout the temperature and frequency ranges measured. Conversely, as shown in Figure 10, the resistivity of **5** increases from 300 to 90 K and then suddenly decreases to 6 K independent of the frequency (inset of Figure 10). Concomitantly, the dielectric constant of **5** suddenly decreases below ~90 K. In order to identify the origin of this behavior, we first have to validate the contribution of the magnetic permeability μ derived from the sample itself ($\mu_{comp} = 4\pi\kappa$, where κ is the susceptibility per unit volume and $\mu_1 = 1 + \mu_{comp}$). The dielectric constant ε_1 is inversely proportional to μ. As well as the χ behavior, the magnetic permeability of compound (μ_{comp}) should also decrease below T_N, so if the magnetic permeability was the cause of the inflection, ε_1 should increase at T_N. In fact the contrary is the case. Namely, this inflection behavior at ~90 K bears no relationship to μ_{comp} (hence, $\mu = 1$ was fixed to derive σ_1 and ε_1) and is an essential phenomenon of the electron transport properties of **5**. Thus, the inflection temperature of conductivity and dielectric constant, interestingly, corresponds to T_N. It should be noted that the intralayer ferromagnetic long-range order also occurs at around T_N to produce intralayer magnetic domains that derive a large dipole need for the antiferromagnetic order between layers. In the present system, the conduction electrons could be carried by an electron transfer hopping between [Ru_2] units via $TCNQR_x^{\bullet -}$ and, hence, scattered by local magnetic spins at the paramagnetic phase *if the hopping electron is interacting with local spins*. Meanwhile, the spin order suppresses spin scattering for the electron transport even in the hopping electron-transfer mechanism. At this time, ε_1 should also be decreased. Thus, the decrease of ρ_1 and ε_1 at the temperatures below T_N are closely associated with the magnetic ordering. Simply put, the transport electrons are interacting with ordered spins in **5**.

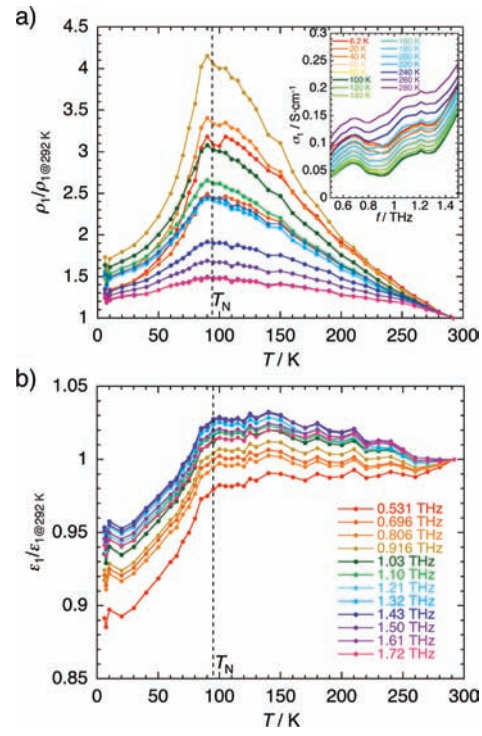

Figure 10. Normalized resistivity (ρ_1, a) and dielectric permittivity (ε_1, b) of **5** as a function of temperature measured at several frequencies by THz-TDS, where the dashed line represents $T_N = 95$ K of **5** estimated by the magnetic data. Inset of (a): THz frequency dependence of σ_1 measured at several temperatures.

Charge Transfer in the Present Series. To ascertain the nature of charge transfer in the system, powder reflection spectra of all compounds were measured (Figure 11 as a function of energy unit of eV). The absorption in the wide range of 2−3 eV in the Ru series (Figure 11a) includes the contribution of the $\pi-\pi^*$ transition of $TCNQR_x^{\bullet -}$. All compounds, even **1** and **2** that present no virtual charge transfer, exhibit such a transition (indeed, all compounds are dark green in color). This fact indicates that the photoexcited charge transfer and/or meaningful π-back-donations from [$Ru_2^{II,II}$] to $TCNQR_x$ occur to induce such a subsequent transition. Indeed, the absorption at 0.8−1 eV is probably due to the charge transfer from [$Ru_2^{II,II}$] to $TCNQR_x$ (unfortunately, energy values distinguishing **1**−**5** could not be

(41) (a) Kida, N.; Hangyo, M.; Tonouchi, M. *Phys. Rev. B* **2000**, *62*, R11965. (b) Pimenov, A.; Tachos, S.; Rudolf, T.; Loidl, A.; Schrupp, D.; Sing, M.; Claessen, R.; Brabers, V. A. M. *Phys. Rev. B* **2005**, *72*, 035131. (c) Pimenov, A.; Biberacher, M.; Ivannikov, D.; Loidl, A.; Mukhin, A. A.; Goncharov, Y. G.; Balbashov, A. M. *Phys. Rev. B* **2006**, *73*, 220407.

(42) Nagashima, T.; Takata, K.; Nashima, S.; Harima, H.; Hangyo, M. *J. Appl. Phys.* **2005**, *44*, 926.

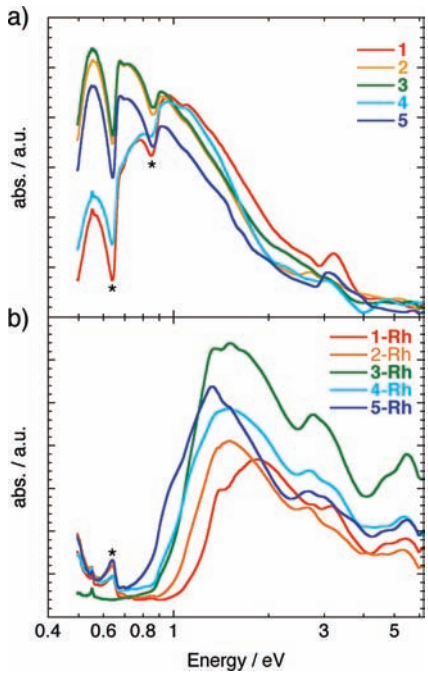

Figure 11. Absorption spectra of **1**−**5** (a) and **1-Rh**−**5-Rh** (b) measured on powder pellets diluted with $BaSO_4$ (∗ indicates nonessential reflection).

evaluated), and this absorption in the Rh series can be found at higher energies of 1.2−1.9 eV (**1-Rh** has the highest energy of 1.9 eV). Interestingly, only **1** and **4** do not exhibit a distinct absorption at lower energy less than 1 eV; likewise for the Rh series. In other words, the nature of **2**, **3**, and **5** should be associated with transitions occurring at lower energies, which would be due to a charge transfer between mixed-valence states (intervalence charge transfer; IVCT) of $[Ru_2]^0 \leftrightarrow [Ru_2]^{\delta+}$ via $TCNQR_x^{\delta-}$. Considering the activation energy $E_a \approx 0.2-0.3$ eV evaluated from the electrical resistivity measurements, the main contributor in the electron transport of the Ru series may be this IVCT. Of course, this IVCT becomes possible by occurring prior to the charge transfer of $[Ru_2^{II,II}] \rightarrow TCNQR_x$, which is tuned by the electron affinity of $TCNQR_x$.

Concluding Remarks

The homologous series of 2-D network compounds $[\{Ru_2(O_2CCF_3)_4\}_2(TCNQR_x)]$ (R_x = H_4, **1**; Br_2, **2**; Cl_2, **3**; F_2, **4**; F_4, **5**), where the $[Ru_2(O_2CCF_3)_4]$ and $TCNQR_x$ units are capable of being electron donor and acceptor, respectively, has been synthesized and structurally characterized. According to the X-ray crystallographic data at 100 K, the two $[Ru_2(O_2CCF_3)_4]$ units cannot be differentiated. The nature of the two precursors allows for a charge transfer from the $[Ru_2^{II,II}]$ unit to $TCNQR_x$ as well as a subsequent charge transfer between mixed-valence $[Ru_2]$ units (IVCT) via $TCNQR_x^{\bullet -}$. In addition, such a charge transfer results in magnetic exchange between $[Ru_2]^{n+}$ units (as $n = 0$, $S = 1$ and as $n = 1$, $S = 3/2$) via $TCNQR_x^{\bullet -}$ with $S = 1/2$. In the present series of compounds, only **5** demonstrates a full charge transfer from $[Ru_2^{II,II}]$ to $TCNQR_x$ to give the formal resonance form $[\{Ru_2^{4.5+}\}\text{-}(TCNQF_4^{\bullet -})\text{-}\{Ru_2^{4.5+}\}]$, whereas other compounds are in the quasi-static state of $[\{Ru_2^{4+}\}\text{-}(TCNQR_x^{0})\text{-}\{Ru_2^{4+}\}]$. These results are consistent with the fact that $TCNQF_4$ has the strongest electron affinity among the presently studied $TCNQR_x$ acceptors. Even in the neutral forms exhibited by **1**−**4**, however, thermally and/or field-activated charge transfers of $[Ru_2^{II,II}] \rightarrow TCNQR_x$ are possibly occurring, as judged by their conductivity properties and the magnetic anomaly observed in **2** and **3**. The ease of thermally and/or field-activated charge transfers is in the order **1** < **4** < **2** ≈ **3**. Thus, the nature of charge transfer is tuned according to **1** < **4** < **2** ≈ **3** ≪ **5** by the electron affinity of $TCNQR_x$ (R_x is H_4, **1**; Br_2, **2**; Cl_2, **3**; F_2, **4**; F_4, **5** in the aromatic ring of TCNQ).

Finally, **5** exhibits 3-D long-range antiferromagnetic order at 95 K and is a semiconductor. This compound constitutes the first instance in which bulk magnetic and conducting properties have been systematically tuned by intramolecular charge transfer. Such a system is likened to a "Creutz-Taube ion expanded to a dimensional lattice". The most exciting result is the discovery that conduction electrons are interacting with localized magnetic spins. The antiferromagnetic transition (or intralayer ferromagnetic transition) at T_N = 95 K accompanies a drastic change of ac conductivity. Obviously, the charge transfer between $[Ru_2]$ units and $TCNQR_x$ plays a key role in the coupling between ordered spins and hopping electrons. Further precise tuning of the energy levels between the HOMO orbital of $[Ru_2]$ unit and LUMO orbital of $TCNQR_x$, namely, making a Class III system at the local level, is needed for the realization of materials in which magnetic-conducting properties are mutually highly cooperative. Work to this end is in progress.

Finally, the present study presents unique materials whose magnetic properties are tunable by intramolecular charge transfers and also demonstrates that the present synthetic strategy employing the charge-transfer resonance scheme is efficient for designing materials with synergy between the magnetic and conducting properties.

Experimental Section

General Procedures and Materials. The TCNQ and $TCNQF_4$ starting materials were purchased from Tokyo Kasei Co. Ltd.: The TCNQ was purified by sublimation before use. The $TCNQR_2$ (R = Br, Cl, F) derivatives were prepared according to literature methods.[43] Solvents were distilled under a N_2 atmosphere using common drying agents. Compounds **1**−**5** were prepared by modification of a synthetic procedure reported previously.[24] All synthetic procedures were performed anaerobically. Compounds **1**−**5** and **1-Rh**−**5-Rh** contain crystallization solvents (see the structural section in the text), some of which are slowly lost at room temperature, so the samples for elemental analyses reflect partial loss and thus a slightly different formula compared to those determined by single crystal X-ray crystallography. Samples aged for a few hours after removal from mother liquids were analyzed for the elemental data, but fresh samples taken immediately from the mother liquids were used for magnetic measurements, resistivity, and THz-TDS measurements.

Syntheses of 1−5. Because **1**−**5** were synthesized according to a common procedure, only the method used for **1** is provided as a representative example. A solution of TCNQ (10 mg, 0.05 mmol) in CH_2Cl_2 (20 mL) was separated into 10 portions and placed into narrow diameter glass tubes (8 mm in diameter), respectively (bottom layer). After this time, a mixed solvent of CH_2Cl_2/*p*-xylene 1:1 v/v (0.5 mL) was added onto the bottom layer as a means to slow the rate of diffusion (middle layer). Finally, a solution (2 mL) of $[Ru_2^{II,II}(O_2CCF_3)_4(THF)_2]$ (80 mg, 0.1 mmol) in *p*-xylene (20 mL) was carefully added onto the middle layer of each batch (top layer). The glass tubes were left undisturbed for 1 week or more to obtain block-type dark-green crystals of **1**·3(*p*-xylene). Elemental analysis (%) calcd for **1**·2(*p*-xylene) $C_{44}H_{24}F_{24}N_4O_{16}Ru_4$: C 30.64, H 1.40, N 3.25. Found: C 30.47, H 1.54, N 3.27. IR (KBr): ν(C≡N), 2238, 2198, 2134 cm^{-1}; ν(C═O), 1641, 1440 cm^{-1}; ν(C═C),

(43) Wheland, R. C.; Gillson, J. L. *J. Am. Chem. Soc.* **1976**, *98*, 3916.

1580w, 1537 cm^{-1}. For **2**, $TCNQBr_2$ (18 mg, 0.05 mmol) was used instead of TCNQ in **1**. Elemental analysis (%) calcd for **2**·(*p*-xylene)·1.7CH_2Cl_2 $C_{37.7}H_{15.4}Br_2Cl_{3.4}F_{24}N_4O_{16}Ru_4$: C 23.57, H 0.81, N 2.92. Found: C 23.85, H 1.10, N 2.91. IR(KBr): ν(C≡N), 2216w, 2198, 2158, 2123 cm^{-1}; ν(C═O), 1645, 1457 cm^{-1}; ν(C═C), 1558, 1487 cm^{-1}. For **3**, $TCNQCl_2$ (14 mg, 0.05 mmol) was used instead of TCNQ in **1**. Elemental analysis (%) calcd for **3**·1.2(*p*-xylene)·2CH_2Cl_2 $C_{39.6}H_{18}Cl_6F_{24}N_4O_{16}Ru_4$: C 25.32, H 0.97, N 2.98. Found: C 25.27, H 1.15, N 3.04. IR(KBr): ν(C≡N), 2223w, 2200, 2161, 2126 cm^{-1}; ν(C═O), 1639, 1461 cm^{-1}; ν(C═C), 1562, 1489 cm^{-1}. For **4**, $TCNQF_2$ (12 mg, 0.05 mmol) was used instead of TCNQ in **1**. Elemental analysis (%) calcd for **4**·2.3(*p*-xylene) $C_{46.4}H_{25}F_{26}N_4O_{16}Ru_4$: C 31.09, H 1.41, N 3.13. Found: C 31.17, H 1.72, N 3.13. IR(KBr): ν(C≡N), 2231w, 2207, 2141 cm^{-1}; ν(C═O), 1640, 1438 cm^{-1}; ν(C═C), 1571, 1561, 1543 cm^{-1}. For **5**, $TCNQF_4$ (14 mg, 0.05 mmol) was used instead of TCNQ in **1**. Elemental analysis (%) calcd for **5**·2(*p*-xylene) $C_{44}H_{20}F_{28}N_4O_{16}Ru_4$: C 29.41, H 1.12, N 3.12. Found: C 29.34, H 1.52, N 3.45. IR(KBr): ν(C≡N), 2217, 2182 cm^{-1}; ν(C═O), 1643, 1441 cm^{-1}; ν(C═C), 1533, 1493 cm^{-1}.

Syntheses of 1-Rh−5-Rh. Compounds **1-Rh**−**5-Rh** were synthesized following the same general procedure. The detailed preparation of **1-Rh** is provided as a representative reaction. A solution of TCNQ (10 mg, 0.05 mmol) in CH_2Cl_2 (20 mL) was separated into 10 portions and placed in narrow glass tubes (8 mm in diameter), respectively (bottom layer). After this time, a mixed solvent of CH_2Cl_2/*p*-xylene 1:1 v/v (0.5 mL) was added onto the bottom layer as a means to slow the rate of diffusion (middle layer). Finally, a solution (2 mL) of $[Rh_2^{II,II}(O_2CCF_3)_4]$ (66 mg, 0.1 mmol) in *p*-xylene (20 mL) was carefully added onto the middle layer of each batch (top layer). The glass tubes were left to diffuse for 1 week or more, which led to block-type greenish purple crystals of **1-Rh**. Elemental analysis (%) calcd for **1-Rh**·2.25(*p*-xylene) $C_{46}H_{26.5}F_{24}N_4O_{16}Rh_4$: C 31.41 H 1.52, N 3.19. Found: C 31.19, H 1.82, N 3.33. IR (KBr): ν(C≡N), 2245, 2226, 2196 cm^{-1}; ν(C═O), 1667, 1460 cm^{-1}; ν(C═C), 1541 cm^{-1}. For **2-Rh**, $TCNQBr_2$ (18 mg, 0.05 mmol) was used instead of TCNQ for **1-Rh**. Elemental analysis (%) calcd for **2-Rh**·1.4(*p*-xylene) $C_{39.2}H_{16}Br_2F_{24}N_4O_{16}Rh_4$: C 25.78, H 0.88, N 3.07. Found: C 25.62, H 1.14, N 3.06. IR(KBr): ν(C≡N), 2228, 2195 cm^{-1}; ν(C═O), 1638, 1460 cm^{-1}; ν(C═C), 1487, 1556 cm^{-1}. For **3-Rh**, $TCNQCl_2$ (14 mg, 0.05 mmol) was used instead of TCNQ for **1-Rh**. Elemental analysis (%) calcd for **3-Rh**·1.4(*p*-xylene)·2CH_2Cl_2 $C_{41.2}H_{20}Cl_6F_{24}N_4O_{16}Rh_4$: C 25.94, H 1.06, N 2.94. Found: C 25.81, H 1.14, N 3.18. IR(KBr): ν(C≡N), 2233, 2198 cm^{-1}; ν(C═O), 1667, 1460 cm^{-1}; ν(C═C), 1562, 1491 cm^{-1}. For **4-Rh**, $TCNQF_2$ (12 mg, 0.05 mmol) was used instead of TCNQ for **1-Rh**. Elemental analysis (%) calcd for **4-Rh**·2(*p*-xylene)·0.3CH_2Cl_2 $C_{44.3}H_{22.6}Cl_{0.6}F_{26}N_4O_{16}Rh_4$: C 29.66, H 1.27 N 3.12. Found: C 29.87, H 1.56, N 3.08. IR(KBr): ν(C≡N), 2239, 2200 cm^{-1}; ν(C═O), 1663, 1460 cm^{-1}; ν(C═C), 1572, 1561, 1543 cm^{-1}. For **5-Rh**, $TCNQF_4$ (14 mg, 0.05 mmol) was used instead of TCNQ for **1-Rh**. Elemental analysis (%) calcd for $[\{Rh_2(O_2CCF_3)_4\}_2(TCNQF_4)]$·*p*-xylene·2.5$CH_2Cl_2$ $C_{38.5}H_{15}Cl_5F_{28}N_4O_{16}Rh_4$: C 29.21, H 0.79, N 2.93. Found: C 224.65, H 1.25, N 3.04. IR(KBr): ν(C≡N), 2246, 2219, 2166 cm^{-1}; ν(C═O), 1667, 1462 cm^{-1}; ν(C═C), 1594, 1545, 1495 cm^{-1}.

General Physical Measurements. Infrared spectra were measured on KBr disks with a Jasco FT-IR 620 spectrophotometer. Powder reflection spectra were measured on pellets diluted with $BaSO_4$ with a Shimadzu UV-3150 spectrometer. Electrical resistivity was measured on a powder-pressed pellet (d = 3 mm ϕ and $l \approx 0.3$ mm) using an Agilent 34420A nanovoltmeter. The pellet sample was in physical contact with two isometric brass plates attached to platinum probe wires. Magnetic susceptibility measurements were conducted with a Quantum Design SQUID magnetometer (MPMS-XL) in the temperature and dc field ranges of 1.8 to 300 K and −7 to 7 T. AC measurements were performed at various frequencies ranging from 1 to 1488 Hz with an ac field amplitude of 3 Oe. Polycrystalline samples embedded in liquid paraffin were measured. Experimental data were corrected for the sample holder and liquid paraffin and for the diamagnetic contribution calculated from Pascal constants.[44]

Terahertz Time-Domain Spectroscopy (THz-TDS). The THz-TDS measurements were carried out covering the frequency range 0.2−2.0 THz with the use of a commercial spectrometer (RT-20000, Tochigi Nikon Co. Ltd.) based on a standard transmission configuration. The powder samples were pressed into a shape of disk with a 3 mm diameter and a 0.2 mm thickness and were placed on a cellophane tape with a 0.05 mm thickness. Measurements were conducted at temperatures below room temperature down to 6 K in a vacuum of 2×10^{-5} Torr. The time-dependent THz waveforms $E(t)$ transmitted through the sample on a cellophane tape, a cellophane tape reference, and in a vacuum at room temperature were changed to respective Fourier transforms $E(\omega)$ (Figure S6 in Supporting Information). Using the measured spectrum, the complex transmission coefficient $t(\omega)$ is defined by $E_S(\omega)/E_V(\omega)$ where $E_S(\omega)$ is the sample spectrum and $E_V(\omega)$ is the vacuum spectrum and written as

$$t(\omega) = t_{VS}t_{SC}t_{CV}\exp\left[i\frac{(n_S - 1)d_S\omega + (n_C - 1)d_C\omega}{c}\right] \quad (1)$$

where $t_{ij} = 2n_i/(n_i + n_j)$ is the complex Fresnel's transmission coefficient at the interface between regions i and j. The subscripts i and j of V, S, and C represent the vacuum, sample, and cellophane tape, respectively, and n_i is the complex refractive index of region i, d_j the thickness of region j, and c the speed of light. n_C is obtained from a separate measurement on the cellophane tape only, and then n_S is obtained by numerically solving eq 1. Finally, the complex dielectric constant $\varepsilon(\omega)$ is evaluated from the relationship

$$\varepsilon(\omega) = \left(\varepsilon_1 + i\frac{4\pi\sigma_1}{\omega}\right) = \frac{n(\omega)^2}{\mu_1} \quad (2)$$

where ε_1 is the real dielectric constant [$\varepsilon(\omega) = \varepsilon_1 + i\varepsilon_2$ and $\varepsilon_2 = 4\pi\sigma_1/\omega$], σ_1 the real conductivity, and μ_1 the magnetic permeability. We assumed μ_1 is 1 because $\chi \ll 1$ although the sample is magnetic substance (see the section regarding THz-TDS in text).

Crystallography. Single crystals with dimensions of 0.15 × 0.13 × 0.10 mm^3 for **1**·3(*p*-xylene), 0.02 × 0.02 × 0.02 mm^3 for **2**·*p*-xylene·2CH_2Cl_2, 0.24 × 0.12 × 0.03 mm^3 for **4**·2.3(*p*-xylene)·1.4CH_2Cl_2, 0.15 × 0.12 × 0.10 mm^3 for **5**·3(*p*-xylene), 0.083 × 0.082 × 0.018 mm^3 for **1-Rh**·3(*p*-xylene), 0.07 × 0.04 × 0.02 mm^3 for **4-Rh**·2.7(*p*-xylene)·0.6CH_2Cl_2, and 0.03 × 0.02 × 0.01 mm^3 for **5-Rh**·*p*-xylene·4CH_2Cl_2 were mounted on cryoloops using Nujol and cooled by a stream of cooled N_2 gas. All measurements were made on a Rigaku Saturn CCD area detector with a graphite monochromated Mo Kα radiation (λ = 0.71070 Å). The structures were solved by direct methods (SHELXL 97, SIR 97, and SIR 92)[45] or heavy-atom Patterson methods[46] and expanded using Fourier techniques (DIRDIF99).[47] Since the crystal of **2**·2CH_2Cl_2 was a non-merohedral twin, where the twin com-

(44) Boudreaux, E. A.; Mulay, L. N. *Theory and Applications of Molecular Paramagnetism*; John Wiley and Sons: New York, 1976; p 491.
(45) (a) Sheldrick, G. M. *SHELXL 97*; University of Göttingen: Göttingen, Germany, 1997. (b) SIR 97; Altomare, A.; Burla, M.; Camballi, M.; Cascarano, G.; Giacovazzo, C.; Guagliardi, A.; Moliterni, A.; Polidori, G.; Spagna, R. *J. Appl. Crystallogr.* **1999**, *32*, 115. (c) SIR 92; Altomare, A.; Burla, M. C.; Camballi, M.; Cascarano, M.; Giacovazzo, C.; Guagliardi, A.; Polidori, G. *J. Appl. Crystallogr.* **1994**, *27*, 435.
(46) PATTY; Beurskebs, P. T.; Admiraal, G.; Beurskens, G.; Bosman, W. P.; Garcia-Granda, S.; Gould, R. O.; Smits, J. M. M.; Smykalla, C. *The DIRDIF program system, Technical Report of the Crystallography Laboratory*; University of Nijmengen, The Netherlands, 1992.
(47) DIRDIF99; Beurskens, P. T.; Admiraal, G.; Beurskens, G.; Bosman, W. P.; de Gelder, R.; Israel, R.; Smits, J. M. M. *The DIRDIF-99 program system, Technical Report of the Crystallography Laboratory*; University of Nijmengen, The Netherlands, 1999.

ponent 1 comprised 51.10% of the crystal, the final R values are less accurate than generally acceptable values. Most non-hydrogen atoms in the main part of the structure were refined anisotropically, while the rest (as crystallization solvents) were refined isotropically because of the presence of disorder. Hydrogen atoms were introduced as fixed contributors. Full-matrix least-squares refinements on F^2 were based on observed reflections and variable parameters, and converged with unweighted and weighted agreement factors of $R1 = \Sigma||F_o| - |F_c||/\Sigma|F_o|$ ($I > 2.00\sigma(I)$), and $wR2 = [\Sigma w(F_o^2 - F_c^2)^2/\Sigma w(F_o^2)^2]^{1/2}$ (all data). All calculations were performed using the CrystalStructure crystallographic software package.[48] The details of crystallographic data for **1**·3(*p*-xylene), **2**·*p*-xylene·$2CH_2Cl_2$, **4**·2.3(*p*-xylene)·$1.4CH_2Cl_2$, **5**·3(*p*-xylene), **1-Rh**·3(p-xylene), **4-Rh**·2.7(*p*-xylene)·$0.6CH_2Cl_2$, and **5-Rh**·*p*-xylene·$4CH_2Cl_2$ are listed in Table 1.

These data have been deposited as CIFs at the Cambridge Data Centre as supplementary publication nos. CCDC-615251 for **1**·3(*p*-xylene), 752263 for **2**·*p*-xylene·$2CH_2Cl_2$, 752264 for **4**·2.3(*p*-xylene)·$1.4CH_2Cl_2$, 615250 for **5**·3(*p*-xylene), 752262 for **1-Rh**·3(*p*-xylene), 752260 for **4-Rh**·2.7(*p*-xylene)·$0.6CH_2Cl_2$, and 752261 for **5-Rh**·*p*-xylene·$4CH_2Cl_2$. Copies of the data can be obtained free of charge by application to CCDC, 12 Union Road, Cambridge CB21EZ, UK (fax: (+44) 1223-336-033; email: deposit@ccdc.cam.ac.uk).

X-ray powder diffraction measurements for **3**, **2-Rh**, and **3-Rh** were conducted on a Rigaku RINT-2500HK diffractometer with Cu Kα radiation ($\lambda = 1.5418$ Å) at room temperature in the range of $5° \leq 2\theta \leq 60°$. A fresh polycrystalline sample was placed in a narrow diameter quartz glass tube with a small portion of mother liquid. Lattice parameters were refined using the LeBail method.[26]

(48) *CrystalStructure 3.15: Crystal Structure Analysis Package*; Rigaku and Rigaku/MSC: The Woodlands, TX, 2000−2002.

Acknowledgment. We acknowledge Mr. T. Izawa and Ms. N. Takahashi at Tokyo Metropolitan University and Mr. N. Shibata at Tohoku University for syntheses of compounds, Prof. T. Akutagawa at Hokkaido University for his pointed advice for the syntheses of $TCNQR_x$, and Dr. S. Takaishi at Tohoku University for measurements of electrical conductivity and helpful discussions. H.M. is grateful for financial support from a Grant-in-Aid for Scientific Research from the Ministry of Education, Culture, Sports, Science, and Technology, Japan (Grant 21350032) and The Asahi Glass Foundation. N.M. thanks the JSPS Research Fellowships for Young Scientists for financial support. K.R.D. thanks Texas A&M University and is grateful for support from the Department of Energy (DE-FG02-02ER45999), the National Science Foundation, and the Welch Foundation (A-1449).

Supporting Information Available: X-ray crystallographic files in CIF format for **2**, **4**, **4-Rh**, and **5-Rh**; structural, magnetic, and spectral data for all compounds. This material is available free of charge via the Internet at http://pubs.acs.org.

JA909489S